Universität für Bodenkultur Wien
University of Natural Ressources and Life Sciences Vienna

Department für Wasser – Atmosphäre – Umwelt
Institut für Wasserwirtschaft, Hydrologie und konstruktiven Wasserbau

The Influence of Catchment Characteristics on Alpine Catchments Under Climate Change

Masterarbeit
zur Erlangung des akademischen Grades Diplomingenieur

Eingereicht von
Moritz Feigl, BSc BSc

Betreuer:
Assoc.Prof. Dr. Matthias Bernhardt

Wien, 2018

Eidesstaattliche Erklärung

Ich erkläre eidesstattlich, dass ich die Arbeit selbständig angefertigt, keine anderen als die angegebenen Hilfsmittel benutzt und alle aus ungedruckten Quellen, gedruckter Literatur oder aus dem Internet im Wortlaut oder im wesentlichen Inhalt übernommenen Formulierungen und Konzepte gemäß den Richtlinien wissenschaftlicher Arbeiten zitiert, durch Fußnoten gekennzeichnet bzw. mit genauer Quellenangabe kenntlich gemacht habe.

Moritz Feigl, Juni 2018

Acknowledgements

First of all, I want to thank my friends and family who supported me during my work on this thesis. Special thanks goes to my brother Michael and my friends, Victor Pauser and Ting Ting Wang, who always spend time prove-reading the things I wrote.

Furthermore, I want to thank Michael Weber for the wonderful cooperation and that he never hesitated to provide advice for handling the problems I faced in this thesis.

I also like to thank my supervisor Dr. Matthias Bernhardt, who gave me the opportunity to work on this topic and who introduced me to the problems of snow hydrology and showed me its importance.

Lastly, I want to thank Martha Marko for listening to my thoughts and problems and for always keeping me motivated throughout this work.

Abstract

Assessing climate change impact on Alpine catchments is necessary, since they are providing many densely populated regions with fresh water. For that, it is important to understand its impact on alpine catchments with different catchment characteristics, but the same climatic inputs.

The aim of this thesis is to derive a methodology to assess the variability of climate change impact due to catchment characteristics and to investigate the influence of aspect. A physically-based hydrological model, the Cold Regions Hydrological Model (CRHM) is used to model the high alpine research catchment Zugspitze. Hydrological response units (HRUs) are delineated using a combination of cluster analysis of physiographic properties of the catchment and natural patterns in the snow cover from a principal component analysis. To investigate the influence of aspect on the climate change impact, the same catchment was "rotated" three times by 90° to create three additional catchments with different aspects. CRHM was used to model an observation period (1980-2015) and a scenario period (2070-2100) for all 4 catchments. For the scenario period, WETTREG data (SRES A1B) was used as meteorological input.

The results show that aspect possibly influences climate change impact on snow melt on a monthly aggregated level. Both by shifting the peak month and by changing the monthly accumulated melt rate. In snow accumulation processes on the other hand, only a minor influence of aspect on the climate change impact could be observed.

Kurzfassung

Die Untersuchung des Einflusses des Klimawandels auf alpine Einzugsgebiete ist notwendig, da diese viele dicht besiedelte Gebiete mit Wasser versorgen. Deshalb ist es wichtig zu verstehen, wie sich die Auswirkungen des Klimawandels bei Gebieten mit unterschiedlichen Gebietscharakteristika aber dem selben klimatischen Input unterscheidet.

Das Ziel dieser Arbeit ist es, eine Methode zur Untersuchung dieses Einflusses zu entwickeln und den Einfluss der Auswirkungen des Klimawandels bei unterschiedlicher Exposition zu untersuchen. Dafür wurde ein physikalisch basiertes hydrologisches Modell, das Cold Regions Hydrological Model (CRHM) verwendet, um das hoch-alpine Einzugsgebiet Zugspitze zu modellieren. Die dafür benötigten Hydrological response units (HRUs) wurden mithilfe einer Kombination aus Clusteranalyse der physiographischen Eigenschaften des Gebiets und den Mustern in der Schneedecke aus einer Hauptkomponentenanalyse ermittelt. Das Einzugsgebiet wurde 3 mal um 90° "gedreht", um 3 weitere Einzugsgebiete mit unterschiedlicher Exposition zu simulieren. CRHM wurde benutzt um eine Beoachtungsperiode (1980-2015) und eine Szenarioperiode (2070-2100) für alle 4 Einzugsgebiete zu modellieren. Für die Szenarioperiode wurden WETTREG daten (SRES A1B) als klimatisches Input verwendet.

Die Ergebnisse weisen auf einen möglichen Einfluss der Exposition auf die monatlich akkumulierten Schmelzraten hin. Durch die unterschiedliche Exposition kommt es zur Verschiebung des Monats mit der maximalen Schmelzrate und zu unterschiedlichen monatlichen akkumulierten Schmelzraten. Bei Schneeakkumulierungsprozessen konnte im Gegensatz dazu nur ein sehr geringer Einfluss der Exposition beobachtet werden.

Contents

1 Introduction **10**

2 Test site and data **14**
2.1 Research catchment Zugspitze 14
2.2 Meteorological input data 16
2.3 Data preprocessing of meteorological data 17
2.3.1 Computation of short-wave radiation 18
2.3.2 Computation of incoming long-wave radiation 19
2.3.3 Correction of precipitation measurements 21
2.4 Natural snow cover patterns 21

3 Methods **24**
3.1 Cold regions hydrological model 24
3.1.1 Model components 25
3.1.2 Modules 25
3.1.3 snobalCRHM 27
3.1.4 Data requirements and interpolation 30
3.2 HRU delineation 30
3.2.1 Data processing 31
3.2.2 Clustering algorithm 34
3.2.3 Clustering 36
3.2.4 Cluster validation with natural snow cover patterns 37
3.2.5 Chosen HRUs and rotated catchments 39
3.3 Analysis tool 41
3.3.1 Hydrological modelling 41
3.3.2 Analysis of multiple model outputs 43

4 Results **46**
4.1 Evaluation of HRU delination method 46
4.2 Influence of aspect on climate change trend 49
4.2.1 Mean peak snow water equivalent 49
4.2.2 Melt rate 50
4.2.3 Snow cover duration 52

5 Discussion and outlook **53**

References **56**

List of Tables

1 HRU parameters 40

2 Aspect (°) of rotated catchments 40

3 Snow indices and model efficiencies for models with different HRU numbers for clustering (12, 10, 8) and the 4 HRUs from Weber et al. (2016), for the years 1998-2016. 46

4 Mean peak SWE (mm), 4°C scenario 49

5 Mean accumulated melt rate (mm), 4°C scenario 51

6 Mean snow cover duration (mm), 4°C scenario 52

List of Figures

1 Potential seasonal changes in stream discharge for different climate scenarios of the Athabasca River Watershed (Neupane et al. 2017). The discharge is given as percentage of the total yearly discharge. 11
2 Importance of mountains as "Water Towers" of the world (Viviroli et al., 2007) 11
3 Zugspitze catchment, (Weber, 2013) 15
4 a) Mean annual temperature and, b) mean annual precipitation sum of the Zugspitze catchment 16
5 Comparison of the calculated and measured long-wave radiation at the DWD station (Weber, 2013) 20
6 Example for corrected precipitation measures(Weber et al., 2018) 21
7 Zugspitze catchment with area used for deriving natural snow cover patterns (Weber et al., 2018) 22
8 Values of the 1., 2., and 3. principal component of the accumulation, ablation, and settlement period. Coordinates given in UTM WGS84 Zone 32N. (Weber et al., 2018) 23
9 1. Principal component of the accumulation period (Weber et al., 2018) . . . 23
10 Example for CRHM model structure (Pomeroy & Kapphahn, 2009) 26
11 Conceptual diagram of the SNOBAL model (Marks et al., 1998) 29
12 Input Data: a) 5m Digital Elevation Model, b) Vegetation data 31
13 Topographic parameters of the Zugspitze:a) slope, b) aspect 32
14 Mean sheltering index 33
15 Resulting HRUs with a) 7 cluster, b) 8 cluster, c) 9 cluster, 10 cluster 37
16 a) clustering result with 10 HRUs, b) HRUs in PCA covered area 38
17 Chosen clustering result with 10 HRUs 39
18 Analysis tool opening screen 42
19 Analysis tool - Choosing climate change trend 42
20 Tables and interactive plots for a) mean peak SWE, b) mean accumulated snow melt, c) mean snow cover duration 44
21 CRHM analysis a) 1980-2015 Panel seasonal plots, b) 1980-2015 Panel monthly plots, c) 2070-2100 Panel seasonal plots, d) 2070-2100 Panel monthly plots . 45

22 Comparing measured and with 10 HRU ("best fit") modelled snow depths results at the a) DWD station (NSE = 0.78), b) LWD station (NSE = 0.72) 47
23 Snow cover results of highest HRU from a) 4 HRUs model by Weber et al. (2016), b) 10 HRU "best fit" model 48
24 Range of values for the three snow indices and runoff for 8, 10 and 12 HRUs. a) Maximum snow water equivalent (MSWE) (mm), b) Day of MSWE (day of year), c) Snow cover duration (days) d) Mean monthly catchment runoff, averaged over 18 years. The bold black lines show the values of the 10 HRU "best fit" model. 48
25 Mean monthly peak SWE for scenario with 4°C increase for HRU 2 50
26 Mean monthly peak SWE for scenario with 5°C increase for HRU 7 50
27 Monthly accumulated melt rate (mm) for 4°C scenario, with shifted peak due to aspect change, for a) HRU 9, b) HRU 1 51
28 Monthly accumulated melt rate (mm) for 4°C scenario, with shifted peak due to aspect change, for HRU 3 52
29 Mean monthly snow cover duration (mm) for 4°C scenario for a) a very steep HRU, b) a flat HRU 53

1 Introduction

The presented thesis investigates how catchment characteristics of an alpine catchment can influence its response to climate change. To examine this, an approach which investigates the influence of one catchment characteristic on the cold regions hydrological processes is applied. Hereby, a first hypothesis can be proposed and also the methodology for future investigations on this problem can be derived.

The Intergovernmental Panel on Climate Change (IPCC) predicted in its Fifth Assessment Report (AR5), that the increase of global mean surface temperature, for 2081-2100, will likely be in the range of $0.3 - 4.8°C$, relative to 1986-2005 (lowest prediction for RCP2.6 and highest prediction for RCP8.5). The snow cover of the northern Hemisphere, which was already observed to be decreasing in the last century, will further decrease (IPCC, 2013). Furthermore, mountain climates are especially vulnerable to climate change (Kohler et al., 2014) due to feedback mechanisms in the climate system (Viviroli et al. 2011). Additionally, there is growing evidence that high mountain environments experience more rapid changes in temperature than environments at lower elevations (Mountain Research Initiative EDW Working Group, 2015).

Snow dominated mountain catchments are characterized by the storage of precipitation as ice and snow during winter and following higher discharge, due to snow melt in summer. This favourable redistribution of discharge to the summer months, when water demand is usually higher, will change with the ongoing global warming (Viviroli et al., 2011) and may result in severe effects for people relying on these water resources. It is already known, that the influence of a warming climate in snow dominated catchments, will reduce the summer runoff and increase the winter runoff due to early melting or rain- instead of snowfall (Etter et al., 2017; Klein et al., 2016; Serquet et al., 2011; Beniston et al., 2017; Neupane et al., 2017; Huss et al., 2017). This effect can for example be seen in the results of the study on the Athabasca River watershed by Neupane et al.(2017). In this study, stream discharge for 2081-2099 was simulated using three Special Report on Emission Scenarios (SRES-B1, -A1B, -A2) and produced the results as seen in figure 1. In each scenario the discharge in summer is reduced and the discharge mainly in spring increased, due to the early melt of snow.

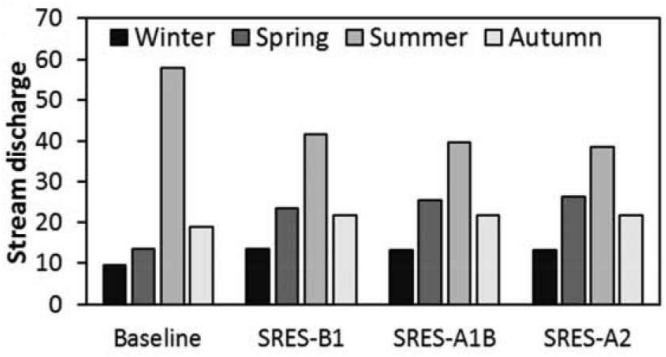

Figure 1: Potential seasonal changes in stream discharge for different climate scenarios of the Athabasca River Watershed (Neupane et al. 2017). The discharge is given as percentage of the total yearly discharge.

Mountain catchments not only provide a favorable temporal redistribution of winter precipitation to spring and summer, but also contribute disproportionately high runoff and reduce the variability of flows in adjacent lowlands (Viviroli and Weingartner, 2004). Viviroli et al. (2007) already showed the areas of the world where high water demand in combination with disproportional mountain runoff formation relative to average lowland runoff occurs. These can be seen in figure 2.

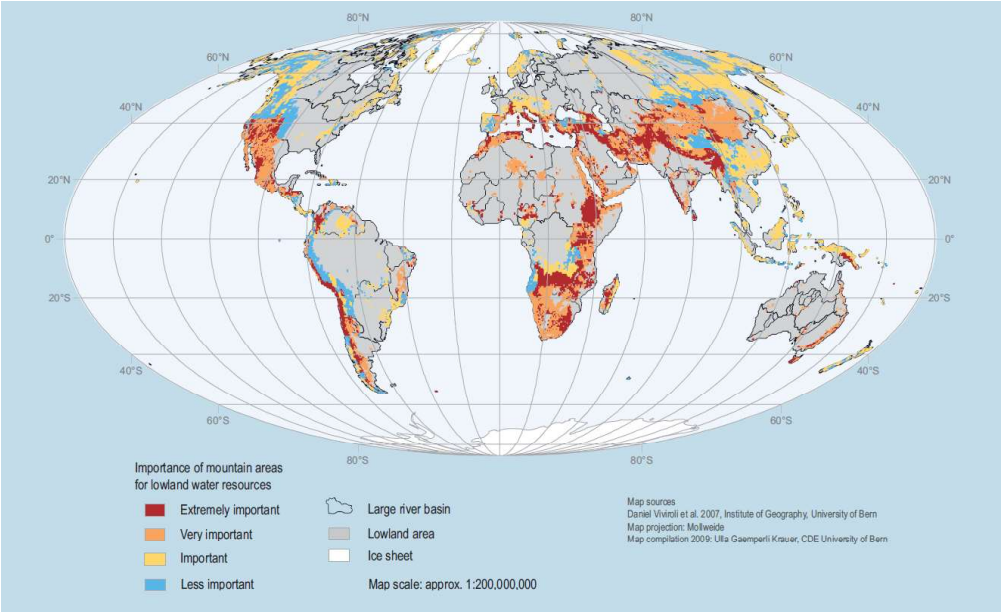

Figure 2: Importance of mountains as "Water Towers" of the world (Viviroli et al., 2007)

In the case of changes in the mountain hydrological systems due to climate change, areas with the combination of high water demand and disproportional runoff from mountains are especially at risk of water supply shortage. Figure 2 shows that some of the most densely

populated regions rely on mountain water resources.

With the possible hydrological changes in alpine catchments and the Earth's ongoing population growth, it will be of great importance to future water management to be able to understand and predict the influence of climate change on alpine catchments better. There are already many studies that investigate the impacts of climate change in alpine catchments: e.g. Huss et al. (2017) gives an overview of the state of research on the cryosphere in mountain regions under changing climate, Beniston et al. (2017) give an extensive overview on the research of the European mountain cryosphere. Nevertheless, there is still a need to further improve our understanding of the environmental and ecological systems in mountain regions, to be able to inform sustainable decision making (Huss et al., 2017).

The underlying problem of this thesis is the following: Is it possible to draw conclusions about the influence of climate change on an alpine catchment from the results of an adjacent catchment with the same climatic input? Or do different catchment characteristics influence the hydrological processes in a way, that leads to different changes? Mountains feature high climate variability caused by strong altitude gradients and exposure to solar radiation (Viviroli et al., 2011). Also mountain snowpacks show large spatial and inter-annual variability, caused by the influence of topography, which can affect temperature gradients, distribution of precipitation, impact of incoming solar radiation and local effects on wind direction and speed (Lopez-Moreno et al., 2013). Previous studies already suggested that snowpack may respond differently in adjacent areas (Uhlmann et al., 2009) and emphasized on the importance to investigate the influence of local topography on the impact of climate variability (López-Moreno et al.,2014).

To determine the influence of climate change on the cold regions hydrological cycle, a physically based hydrological model which fully describes the cold regions hydrological processes is necessary (Rasouli et al., 2014). The Cold Regions Hydrological Model (CRHM) (Pomeroy et al., 2007), which is a physically based flexible model assembly system, includes all necessary cold regions hydrological processes and is deemed suitable for this investigation. CRHM was already used to successfully model the hydrological processes in a wide range of different catchments globally. There are studies in Canada (Dornes et al., 2008; Fang and Pomeroy, 2008; Ellis et al., 2010; Mahmood et al., 2017, Cordeiro et al., 2017; Krogh et al., 2017), in western China (Zhou et al., 2014), Patagonia (Krogh et al., 2014), the German

Alps (Weber et al., 2016) and the Spanish Pyrenees (López-Morenoet al., 2013; Rasouli et al., 2014). Additionally, CHRM was evaluated in the SnoMIP2 snow model comparison, and performed relatively well (Rutter et al. 2009).

CRHM simulates the hydrological cycle for hydrological response units (HRUs). The concept of HRUs (Leavesley et al., 1983; Flügel et al., 1993) separates the catchment in areas that are homogeneous with respect to their hydrological responses. This makes the calculation by single sets of parameters, state variables, and fluxes, including horizontal fluxes, possible (Pomeroy et al. 2007). To adequately delineate HRUs in this investigation, a clustering approach coupled with a principal component analysis (PCA) of snow depth was applied. This approach uses patterns found in the PCA analysis method by Weber et al. (2018), to choose the most suitable number of HRUs from the cluster analysis. The cluster analysis uses information about elevation, slope, aspect, an wind sheltering index and vegetation to divide the investigation catchment into HRUs. The modelling results of this HRU delineation approach are then compared to the modelling results of the same catchment from a publication of Weber et al. (2016), to quantify its influence on the hydrological modelling. This method was developed to minimize the subjective choices that are associated with usual HRU delineation procedures. It would also allow a better comparison between modelling results of different catchments for future investigations.

To simulate catchments with different catchment characteristics and the same climate input, the investigation catchment is rotated by 90° three times. This results in 3 additional catchment versions with changed aspect. Changing the aspect of a catchment results in a different energy balance, due to changes in solar radiation input. Previous studies already showed that the snowpack thermodynamic is strongly influenced by aspect and it influences both snow accumulation and melting (Hinckley et al., 2012).

The whole investigation will be conducted at the high mountain Research Catchment Zugspitze, in Germany. On this catchment, past (1980-2015) and future (2070-2100) snow cover development will be investigated. For the future time period the climate input will be taken from the WETTREG project (Wetterlagen-basierte Regionalisierungsmethode, version 2006) (Enke and Kreienkamp 2006 a-d). The WETTREG method is a statistical regionalization method, based on the ECHAM5/OM GCM and scenario run 1 (SRES A1B, A2, B1). The WETTREG data temperature, which has a trend of 2.72 °C for the period 2020-2100,

will be modified to induce different trends on the temperature data. This is done by using a linear model to adjust the temperature time series to trends of 3, 4 and 5 °C. This allows the investigation of the influence of different future temperature trends. For analysis of the modelling output for the investigation catchment and the additional 3 rotated catchments, an analysis tool was developed in the R package *Shiny* (Chang et al. 2017). This app is used to interpolate the meteorological data to the HRUs, to prepare and start the CRHM modelling procedure and to analyze the results.

2 Test site and data

2.1 Research catchment Zugspitze

The research catchment Zugspitze is part of the Wetterstein massif and located in the Northern Calcareous Alps. The catchment is situated in Germany at the German-Austrian border, centered at UTM 5250416 N 653692 E (Weber et al., 2016). It has an area of 12.7 km^2, a mean elevation of 2229 m a.s.l., with Zugspitze Mountain (2962 m a.s.l.) as the highest and the gauge station Partnach spring (1365 m a.s.l.) as the lowest point.

The vegetation of the catchment can be classified into 4 zones: the subalpine Krummholz-zone (>2000 m a.s.l.), the alpine zone (2000-2400 m a.s.l.) with sedges, the subnival zone (2400-2700 m a.s.l.) with pioneer plants and the nivale zone (>2700 m a.s.l.) (Friedmann und Korch, 2010). The geology of the catchment is characterized by 220 mil. year old 600-800 m thick Wetterstein limestone. Underneath lies the 300-400 m thick Partnach layer (marly claystone) which serves as an aquiclude (Miller, 1962). The catchment is dominated by numerous karst formations such as dolines and ponors and shows typical forms of glacial erosion and accumulation (Weber, 2013). There are two glaciers remaining in the catchment, the Northern Schneeferner (nördlicher Schneeferner) with an area of 0.21 km^2 (2015) and the Southern Schneeferner (südliche Schneeferner) with an area of 0.034 km^2 (2015) (Hagg, 2018). Both were once part of the Schneeferner glacier, which diminished in size since the second half of the 19th century and very drastically since the 1970s (Hagg et al., 2012).

Due to the catchment being karstified, there is almost no surface run-off, only in cases of high rainfall intensities (Weber, 2013). However, Rappl et al. (2010) showed, that there is no significant underground leaking to adjacent catchments and it can therefore be assumed

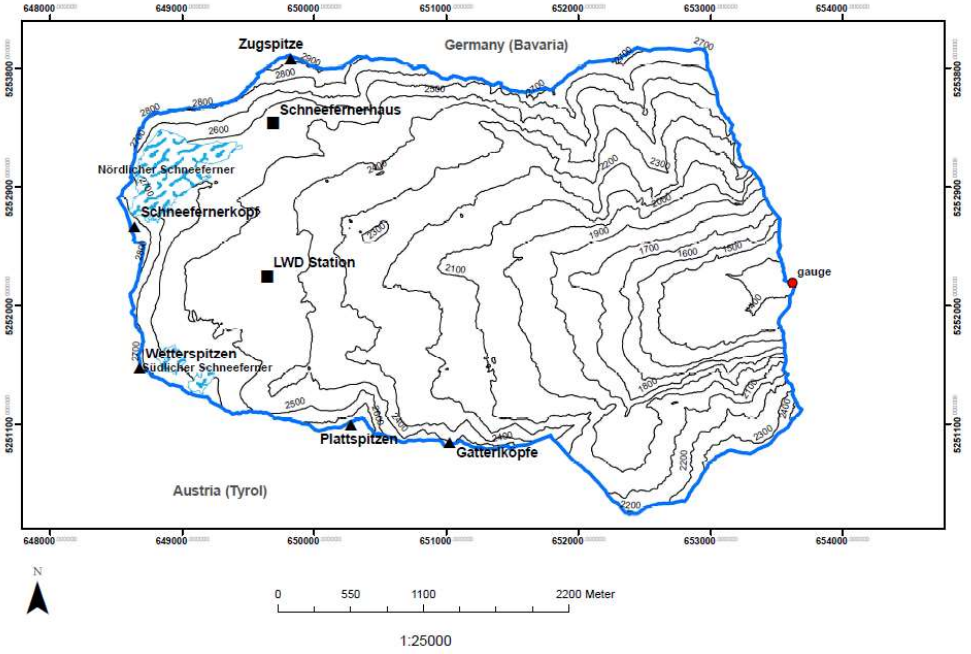

Figure 3: Zugspitze catchment, (Weber, 2013)

that the gauging station measures all discharge from the catchment.

Meteorological measurements from the Wetterhütte Zugspitze of the DWD (German Weather Service) (see figure 3) are available since 1900. The mean annual temperature for the time span 1900-2017 is -4.6 °C. The corresponding time series can be seen in figure 4a. Fitting a simple linear model on the data reveals a positive temperature trend over the whole time span. Comparing the mean annual temperature of the years 1901-1911 with -5.22 °C to the mean of 2007-2017 with -3.66 °C, a increase of 1.56 °C is apparent. The mean annual precipitation sum for the time span 1900-2017 is 1780.9 mm/yr. The corresponding time series can be seen in figure 4b. A positive trend can also be seen in the the precipitation time series. Here the mean annual precipitation sum of the years 1901-1911 is 1405.84 mm/yr, while in 2007-2017 it increases to 1992.08 mm/yr, leading to an increase of about 586 mm/yr. Therefore, a change in the climate of the catchment is already visible over the last 117 years. This change, with a temperature increase of 1.56 °C changed the amount of precipitation significantly and reduced the area of the Northern Schneeferner by 80% and the Southern Schneeferner by 96% (Hagg, 2018). These changes suggest that a predicted temperature increase of 4-5 °C could have tremendous impact on the catchment.

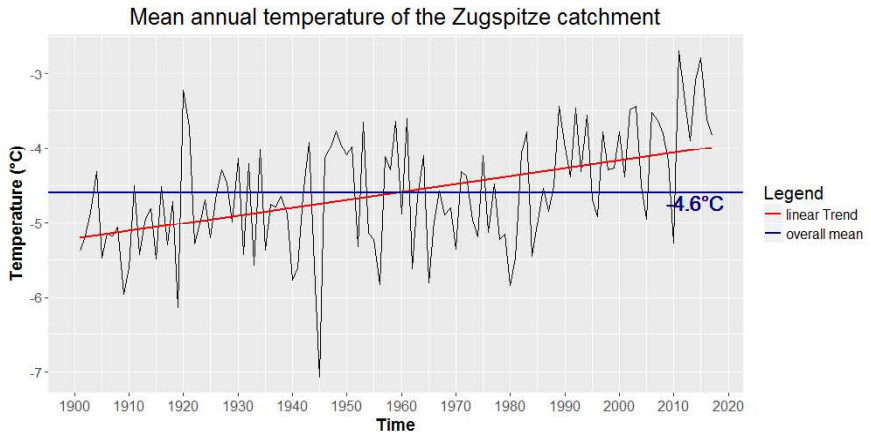

(a)

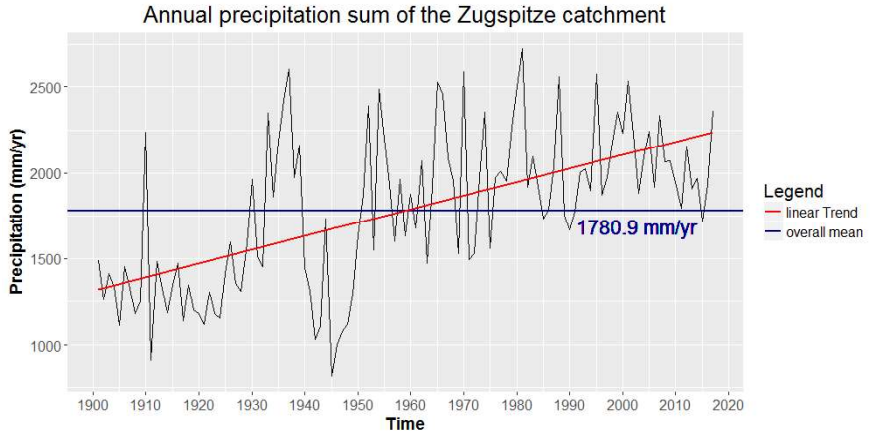

(b)

Figure 4: a) Mean annual temperature and, b) mean annual precipitation sum of the Zugspitze catchment

2.2 Meteorological input data

The historic meteorological date as basis for the CRHM modelling, was taken from the Wetterhütte Zugspitze (see figure 3) of the DWD (German Weather Service), which is located at an elevation of 2964 m a.s.l.. It consists of air temperature, precipitation, wind speed, relative humidity, dew point, sunshine duration and information about the cloud cover for the years 1980-2016 in hourly or daily (precipitation and cloud cover) time steps. Additionally, there is long-wave radiation data available for a short time period. This will be used to validate calculated long-wave radiation in section 2.3. For using the DWD as input for the Cold Region Hydrological Model, the data had to be preprocessed to delete measurement errors and fill in missing data. This is described in section 2.3. Since 1998 the DWD also measures snow depth. This was used to validate the modelling results.

An additional historical data set was used for validation of the precipitation data: the data from the LWD (Lawinenwarndienst Bayern) station. This station is in operation since 1998 and collects temperature, relative humidity, long-wave radiation, short-wave radiation, wind, precipitation and snow parameters (e.g. snow height, snow water equivalent SWE). All measurements are taken in 10 min intervals. It is not used for modelling purposes, as it contains too large gaps, with many summer months missing.

For the climate change scenario runs, the WETTREG (Wetterlagen-basierte Regionalisierungsmethode, version 2006) (Enke und Kreienkamp, 2006 a-d) data was used. WETTREG is a statistical regionalization method which relates large-scale circulation conditions, from global climate models (GCMs) or regional climate models (RCMs), to local weather variables (Enke et al., 2005). The WETTREG data is based on the projections by the ECHAM5/OM GCM and scenario run 1(SRES A1B, A2, B1). The WETTREG method is based on the recombination of historical measurements under the condition of the best possible approximation to the frequency distribution of the large-scale atmospheric condition of the GCM (Weber et al., 2016). The output of this method is restricted by the maximum and minimum values of the historical data, which can not be exceeded (Spekat et al., 2007). Unlike other downscaling products, WETTREGs future projection are especially generated for all German DWD stations. As input for the Cold Regions Hydrological Model, the A1B emission scenario was used, where precipitation remains normal (Enke and Kreienkamp, 2006 a-d). WETTREG data was already successfully applied to climate studies in southern Germany like the KLIWA (climate change and consequences for water management)(Blomenhofer et al., 2009, Klämt 2005, 2008; Reich 2005) and also on the Zugspitze basin (Weber et al., 2016).

2.3 Data preprocessing of meteorological data

Weber (2013) already prepared the DWD and LWD data sets and corrected measurement errors (outliers) and filled in missing values. The applied methods will be described shortly, with a focus on the computation of the radiation data, which is an important factor in this investigation.

Outliers were defined as values:

- which were higher or lower than the highest or lowest ever measured values.
- which change per time interval (1 hour) exceeded a certain station specific threshold (11 times the standard deviation).

Identified outliers were removed and treated as missing values. Missing values were filled in with three methods, depending on the length of the gap, from Liston and Elder (2006):

- Gap of 1 hours: Filled with the average of the previous and following hour.
- Gap of 2-24 hours: For each hour take the mean of the same hour of the previous and the following day to preserve the diurnal cycle of the data.
- Gaps >24 hours: An autoregressive integrated moving average (ARIMA) model is used to forecast the missing values.

For the two daily measurements, sunshine duration and precipitation, single missing values were filled by averaging, and longer gaps were filled by linear interpolation. Missing values of cloud cover could not be interpolated by the method of Liston and Elder (2006), because it was not measured between 20:00 and 03:00 o'clock. Therefore the gaps were also filled with linear interpolation. LWD data, which is available in 10 min intervals, was first aggregated to hourly times steps, before performing the data preprocessing.

The short wave radiation Q_{si} and outgoing global radiation Q_{so} of the LWD data set was noise corrected after removing unrealistic values ($> 4000 W m^{-2}$). Noise in the radiation data was defined as values > 0 during night-time. Using the sunshine-hours, those were set to 0.

For modelling the catchment with the Cold Regions Hydrological Model (CRHM) (see section 3.1) also short- and long-wave radiation are necessary inputs, which are calculated from other measurements. Long-wave radiation is available for a short time period in the DWD data set and is used to adjust the calculation. The WETTREG data set does not include radiation data as well and will also be calculated. The following two section will describe this calculations in detail.

2.3.1 Computation of short-wave radiation

The short wave radiation was calculated with a method by Liston and Elder (2006), using the relationship to cloud cover σ_c, temperature T (°C), relative humidity RH (%), slope β

(°), and aspect ξ_s (°).

For this, the cloud cover is estimated by

$$\sigma_c = 0.832 \; exp(\frac{RH_{700} - 100}{41.6}) \qquad (0 \leq \sigma_c \leq 1), \tag{1}$$

using the relative humidity at 700mb (= 3000 m) level RH_{700}. RH_{700} can be calculated using the temperature T_{700} and dewpoint temperature T_{d700} at 700 mb level. They are calculated with the air temperature lapse rate and the dewpoint temperature lapse rate, both taken from Kunkel (1989).

The short-wave radiation $Q_{si}(Wm^2)$ is then calculated with

$$Q_{si} = S \times (\Psi_{dir} \text{cos} i + \Psi_{dif} \text{cos} Z), \tag{2}$$

where S is the solar irradiance at the top at the atmosphere striking a surface normal to the solar beam (= 1370 $Wm^{-}2$, Kyle et al., 1985). i is the angle between direct solar radiation and a sloping surface and Z the solar zenith angle. Ψ_{dir} and Ψ_{dif} are the direct and diffuse fractions of solar radiation reaching the surface. Those can be calculated by

$$\Psi_{dir} = (0.6 - 0.2 \; \text{cos} Z)(1.0 - \sigma_c) \tag{3}$$

$$\Psi_{dif} = (0.3 - 0.1 \; \text{cos} Z)\sigma_c \tag{4}$$

The most important variable in this investigation, the aspect ξ_s, is used to calculate the cosinus of the angle between direct solar radiation and the sloping surface i:

$$\text{cos} i = \text{cos}\beta + \text{cos} Z + \text{sin}\beta \; \text{sin} Z \; \text{cos}(\mu - \xi_s), \tag{5}$$

where also the solar azimuth μ is needed as well.

2.3.2 Computation of incoming long-wave radiation

Long-wave radiation is an important variable in snow modelling, as it is the most important energy source for snow melt (Ohmura, 2001). This parameter is often not measured due to difficulties and costs, but can be calculated using its relationship with vapour pressure,

temperature and cloud cover (Sedlar and Hock, 2009). The calculation of the incoming long-wave radiation is based on the Stefan-Boltzmann law, using a parametrization developed by Konzelmann et al. (1994). For a clear sky, it is defined as

$$\epsilon_{cs} = 0.23 + a(\frac{e}{T})^{\frac{1}{b}}, \tag{6}$$

with the coefficients a = 0.443 and b = 8, e the vapour pressure (mb) and T the temperature (°C). For all-sky conditions, the cloud cover has to be considered. This is done using the parametrization by König-Langlo and Augstein (1994):

$$\epsilon_{eff} = \epsilon_{cs} + aN^p, \tag{7}$$

with the coefficients a = 0.2176, p = 1.5 and N the cloud cover ($\frac{1}{8}$). Sedlar and Hock (2009) found that a combination of both parametrizations produce the best results for estimating the long-wave radiation. This combined approach was applied to the DWD data set. Comparing the calculated long-wave radiation to the measured data showed a reasonably good fit, with an NSE of 0.76. Weber (2013) improved the fit (NSE of 0.81), by selecting the coefficients of equation 6 and 7 with an global optimization algorithm (DDS dynamical dimensioned search, Tolson and Shoemaker, 2007). A comparison of the resulting time series and the measured values can be seen in figure 5. Using these fitted parameters, the long-wave radiation for the WETTREG data was calculated as well.

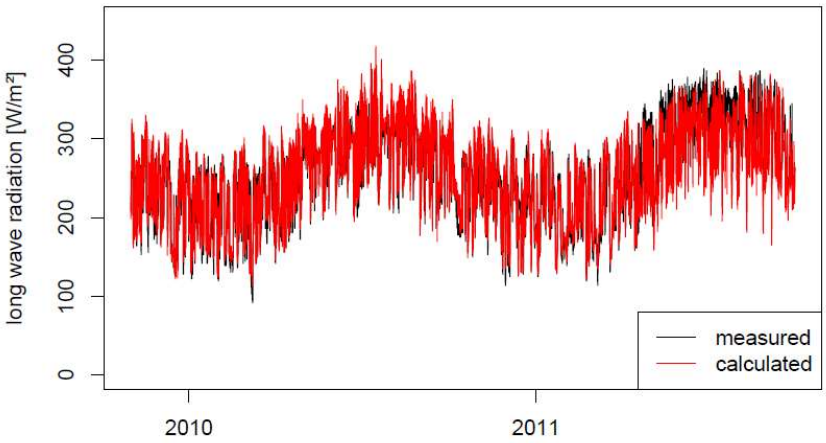

Figure 5: Comparison of the calculated and measured long-wave radiation at the DWD station (Weber, 2013)

2.3.3 Correction of precipitation measurements

Using the LWD station, which measures SWE and precipitation, it was noted that there is a systematic offset between those two measurements. To quantify the offset, the sums of winter precipitation (October - March, main accumulation period) of 2012-2017, excluding days with temperature $> 0°C$, were compared to the SWE measurements for the same time period. This results in a accumulated SWE of 5295 mm and a sum of precipitation of 3544 mm, which is almost exactly 50% difference. This discovery agrees with results published by WMO (2011) and Gross et al. (2017). The LWD station has shown to be largely unaffected by snow redistribution processes and is therefore suited for precipitation correction (Weber et al., 2018). In accordance with these findings, the precipitation data was corrected by multiplying the precipitation data by the factor 1.5, at temperatures $\leq 0°C$ in winter. An example for the corrected precipitation values can be see in figure 6 for the winter 2014/2015.

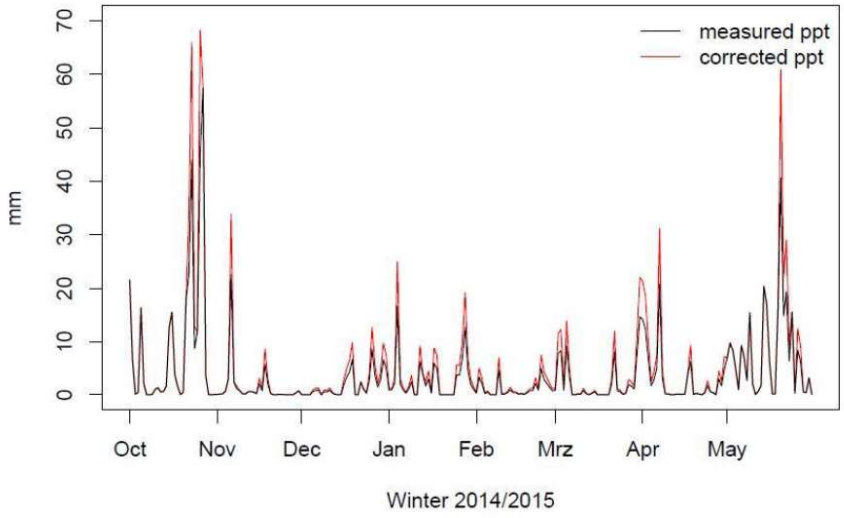

Figure 6: Example for corrected precipitation measures(Weber et al., 2018)

2.4 Natural snow cover patterns

In a parallel study, Michael Weber et al. (2018) identified dominant snow depth patterns on the Zugspitze catchment. These patterns are the results of a principal component analysis (PCA) of the snow depth time series. The snow depth data was obtained by a terrestrial LiDAR (Light Detection And Ranging) system during 15 measurement campaigns from June

2014 to July 2017. Due to the restriction from terrestrial system, measurements were only available for a small part in the south-west of the catchment which can be seen in figure 7. The missing values in the PCA are due to trenches, where the terrestrial LiDAR could not measure. Therefore, also patterns from missing values and the outline of the PCA, are effects of the topographic characteristics of the area.

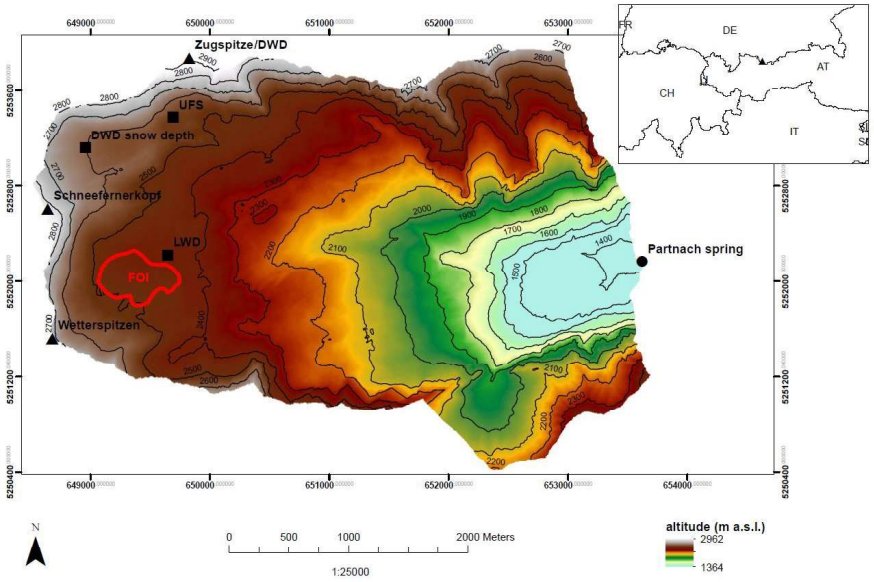

Figure 7: Zugspitze catchment with area used for deriving natural snow cover patterns (Weber et al., 2018)

PCA was applied separately to the accumulation, ablation and the settlement period. The first three principal components (PCs) for each period are shown in figure 8. The most distinct pattern of snow depth distribution can be observed in the accumulation period. Especially the 1. principal component (PC) of the accumulation, shows clear small scale variations (5-20 m), which resemble the snow free surface. Weber et al. (2018) noticed that snow depth distribution is largely defined during accumulation and that it strongly influences processes during ablation and hence runoff generation. The patterns visible in the 1. PC of the accumulation period are shown in more detail in figure 9. They will be used as part of the HRU delineation method applied in this investigation.

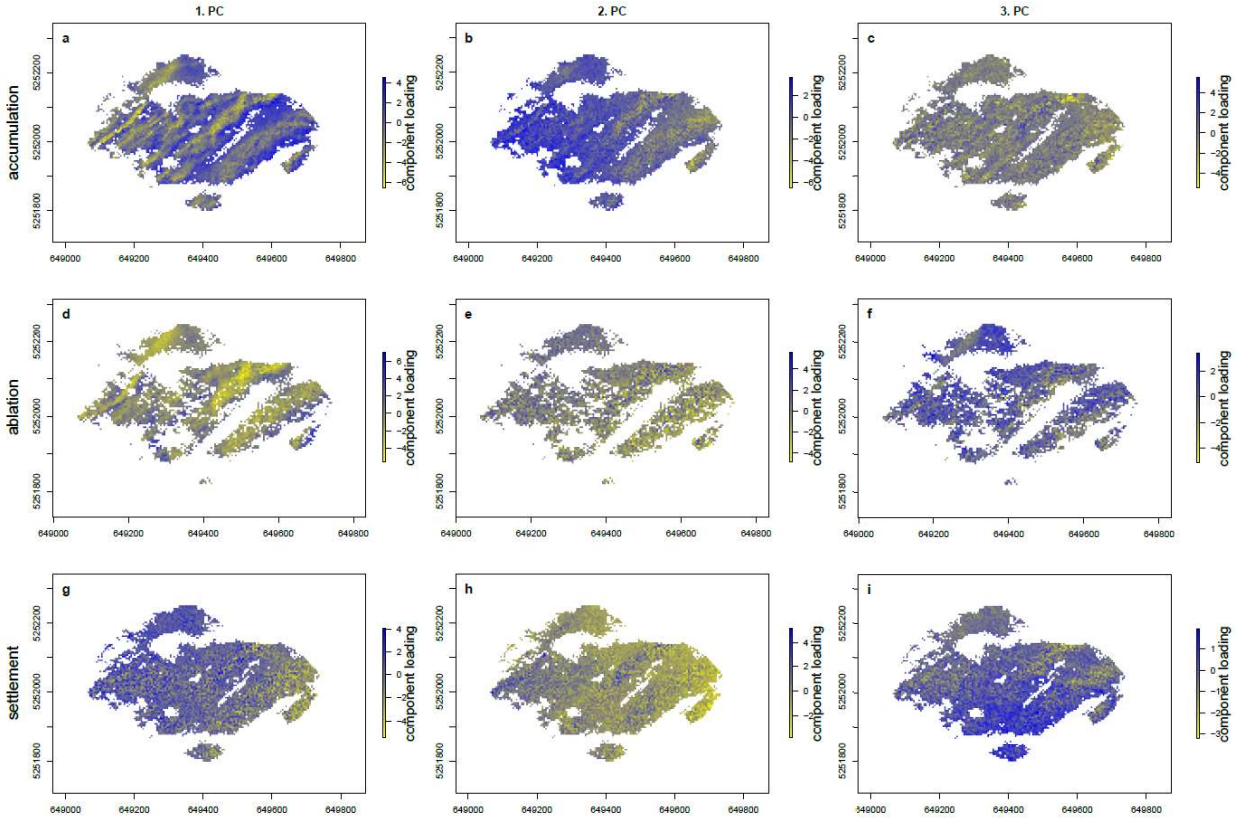

Figure 8: Values of the 1., 2., and 3. principal component of the accumulation, ablation, and settlement period. Coordinates given in UTM WGS84 Zone 32N. (Weber et al., 2018)

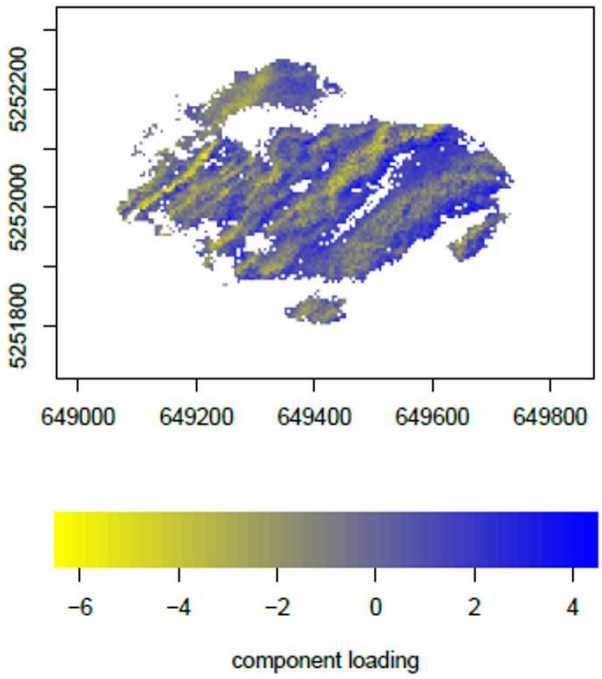

Figure 9: 1. Principal component of the accumulation period (Weber et al., 2018)

3 Methods

3.1 Cold regions hydrological model

CRHM is an object-oriented modelling system, which was designed for small to medium sized basins, with a focus on the cold region aspects of hydrology. It is used for building physically-based hydrological models. Its modular structure permits choosing adequate process modules from a library for simulating the hydrological processes in a catchment. CRHM simulates the hydrological cycle for hydrological response units (HRUs). The concept of HRUs (Leavesley et al., 1983; Flügel et al., 1993) separates the catchment in areas that are homogeneous with respect to their hydrological responses. A more detailed definition is given by Pomeroy et al. (2007), which was used for CRHM. They defined HRUs as spatial units of mass and energy balance calculation, that correspond to biophysical landscape units, within which processes and states can be adequately described for the calculation by single sets of parameters, state variables, and fluxes, but having a place in a landscape sequence or water/snow cascade (Pomeroy et al., 2007). Such biophysical landscape units, state variables and vertical and horizontal fluxes are vegetation cover, soil moisture, evaporation and runoff, respectively. HRUs can have sizes varying from a single agricultural field up to a whole sub-basin. Due to the high level of confidence in the process representation of the modules and good flexibility of model structure, there is diminished need for calibration (Pomeroy et al. 2007).

While the aim of many previous CRHM studies (see section 1) was to predict cold regions hydrological processes with minimal calibration, additional topics were featured, such as: understanding hydrological processes in a catchment, examining the influence of climate change on the hydrological processes, understanding the hydrological response to climate variability, to evaluate CRHM in different environments, and to investigate the impact of snow management as a tool to enhance runoff during droughts. Two studies (López-Moreno et al., 2013 and Rasouli et al., 2014) already used CRHM to investigate the hydrological sensitivity of catchments to climate change, but did not investigate the influence of topography or vegetation.

3.1.1 Model components

CRHM consists of the following components:

- Observations: time-series of meteorological data
- Parameters: parameters describing the HRUs
- Modules: Algorithms describing different processes
- Groups: collection of modules executed in sequence, can be used in place of a specific individual module
- Structure: parallel collection of modules, a group applied to specific HRU
- Variables and States: created by declaration in the modules

Observations are the input data sets for the model. Parameters are chosen individually for each HRU and represent the physical properties. The main task for setting up a CRHM is to choose a set of modules that are needed to describe the catchment processes. For that, groups and structure are ways to use different sets of modules, for different HRUs. For more detailed explanation of the components of CRHM, refer to Pomeroy et al. (2007).

3.1.2 Modules

The CRHM modules can be divided into ten classes:

- Basin
- Observation
- Radiation
- Snow transport
- Interception/Sublimation
- Evapotranspiration
- Snowmelt
- Infiltration
- Soil moisture balance
- Flow

An example of a CRHM structure is shown in figure 10. The selection of modules was taken from the investigation of Weber et al. (2016), which already used CRHM to model the Zugspitze Research catchment. The following list includes all used modules and a short

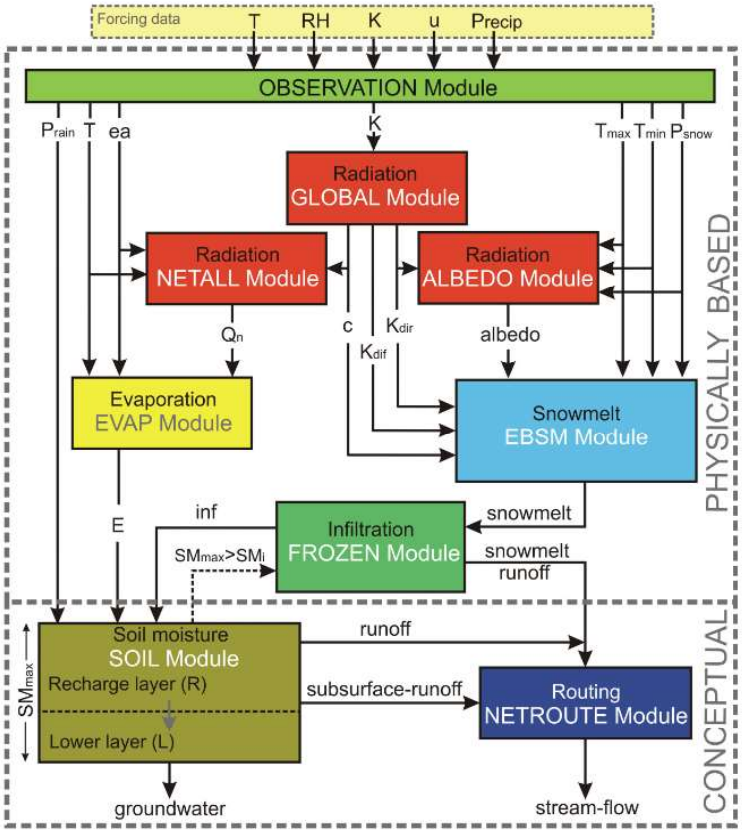

Figure 10: Example for CRHM model structure (Pomeroy & Kapphahn, 2009)

description. Only the module SnobalCRHM, which is used for the main outputs for this investigation, is described in more detail in the next section. For all the other modules, a more comprehensive description can be found in either the publications mentioned, or in Pomeroy et al. (2007). The chosen modules were:

- **Basin**: Sets parameters for describing the basin and HRUs
- **Observation**: Reads in the meteorological data and uses thresholds to calculate the amount of precipitation that comes down as snow.
- **Global**: Calculates the theoretical interval short-wave direct and diffuse solar radiation and the maximum number of daily sunshine hours. Method by Garnier and Ohmura (1970).
- **Netall**: Calculates the Netall radiation with equation by Brunt (1932).
- **albedo_Richard**: Calculates the albedo with an algorithm by Verseghy (1991) modfied by Essery and Etchevers (2004).

- **Calcsun**: Calculates the sunshine hours for each HRU from short wave radiation and the maximum possible sunshine hours provided by the global module.
- **Slope_Qsi**: Is used to adjust the incoming short wave radiation to the slope.
- **CanopyClearing**: Is used to model interception and sublimation. For details refer to Ellis et al. (2010).
- **evap**: Calculates evapotranspiration using a modified Penman-based method for unsaturated evapotranspiration from Granger and Pomeroy (1997).
- **SnobalCRHM**: Module for modeling the snow cover. See section 3.1.3.
- **pbsmSnobal**: This module is used to model the snow redistribution between HRUs. pbsmSnobal is a variation of the original pbsm (prairie blowing snow module), that uses the SWE output from SnobalCRHM. The pbsm is originally by Pomeroy (1989) and was further developed by Pomeroy and Li (2000).
- **frozenAyer**: Calculates infiltration processes. For details refer to Zhao and Gray (1999), Gray et al. (2001).
- **Soil**: Used for calculating the soil moisture balance. For details refer to Fang et al. (2013).
- **Netroute**: This module is used to calculate the water flow between the HRUs and the basin discharge. This is done using the routing method of Clark (1945).

3.1.3 snobalCRHM

The module snobalCRHM is used to calculate the most important outputs for this investigation: snow water equivalent (SWE)(mm), melt rate (mm), and snow depth (m). Therefore, this section will describe snobalCRHM in more detail, to fully understand the influence of catchment parameters (now only aspect) on the calculated outputs. snobalCRHM is based on the snowmelt model snobal, which was first presented by Marks (1988) and described conceptually by Marks et al.(1992), and in great detail by Marks et al. (1998).

Modelling the snow cover is done in snobal, by calculating the energy balance ΔQ of the snow cover. This balance is dependent on the heat exchange at the snow cover and

snow-soil interface (Anderson et al., 1979; Male and Granger, 1981) and drives temperature and vapour density gradients, which in turn cause metamorphic changes and melting (Marks et al., 1998). The energy balance is calculated with:

$$\Delta Q = R_n + H + L_v E + G + M, \tag{8}$$

where R_n, H, $L_v E$, G and M are net radiative, sensible, latent, conductive and advective energy fluxes ($W m^{-2}$). The net radiation is calculated by

$$R_n = R_{n,sol} + I_w - (\epsilon_s \sigma T_{s,0}^4), \tag{9}$$

where $R_{n,sol}$ is the net solar radiation, I_w the solar irradiance and the last term is the Stefan-Boltzmann law, which gives the power radiated from a grey body. Here, the surface emissivity ϵ_s is a constant value of 0.99. From this equation, it is obvious that the solar net radiation, which is directly influenced by the aspect and slope, is a driving force of the energy balance of the snow cover.

The conductive energy fluxes are caused by the energy transfer between the snow cover and the ground. The advective energy fluxes are caused by rainfall and are only calculated when precipitation occurs. The equations for the other fluxes will not be discussed here, as they are not directly influenced by topographic characteristics. A description can be found in Marks et al. (1998).

In case of $\Delta Q = 0$, a thermal equilibrium exists. In case of a negative ΔQ, the snow cover is cooled and its cold content increases. The cold content is the amount of energy in $J m^{-1}$ required to warm the snow cover to $0°C$. In case of positive ΔQ the snow cover gets warmer and the cold content decreases. Positive ΔQ will warm the snow cover until it reaches $0.0°C$, any additional positive ΔQ will produce snow melt. If the amount of liquid water in the snow cover reaches the maximum liquid water holding capacity $w_{c,max}$, it will result in runoff. The maximum liquid water holding capacity is calculated for each time step by (Davis et al., 1985)

$$w_{c,max} = \frac{\text{Volume of water}}{\text{Volume of snow} - \text{Volume of ice}}. \tag{10}$$

Snobal models the snow cover in two separate layers: an active surface layer with defined

thickness and a lower layer. Both have their own specific mass (kgm^{-2}) and temperature $^{\circ}C$. A conceptual diagram of the snobal model can be seen in figure 11.

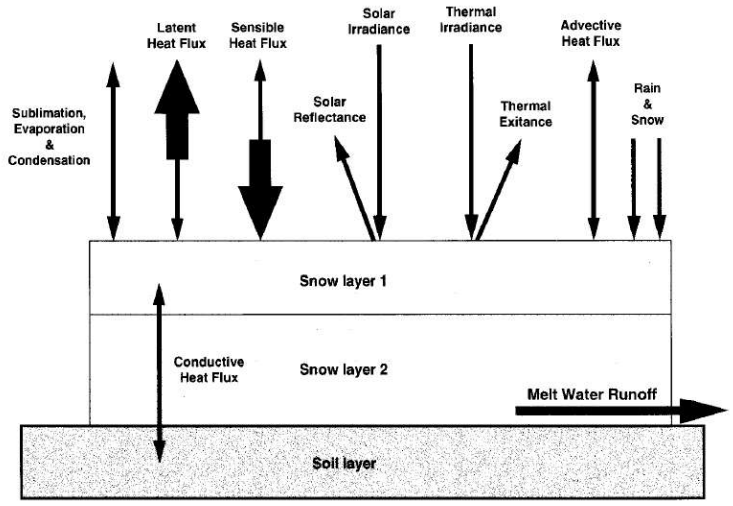

Figure 11: Conceptual diagram of the SNOBAL model (Marks et al., 1998)

The temperature of the surface layer is either taken from initial conditions, or calculated at the end of each time step, while the temperature of the lower layer depends on its snow cover mass (Marks et al. 1998). The layer specific cold content cc_s is calculated using its specific mass, its temperature and the specific heat of ice calculated from the layer temperature. The energy available for melting (Jm^{-2}) is calculated for each layer (shown by the index: 0 = surface, 1 = lower layer) with:

$$Q_0 = \Delta Q_0 \times t_{step} + cc_{s,0} \tag{11}$$

$$Q_1 = (G - G_0) \times t_{step} + cc_{s,1} \tag{12}$$

The available energy for melting the surface layer (Q_0) is a function of the change in energy balance per time step and the cold content ($cc_{s,0}$). The energy for melting the lower layer (Q_1) results from the conductive heat from the ground (G), from the surface layer (G_0) and the cold content ($cc_{s,1}$). In case of negative Q_0 or Q_1 and availability of liquid water, refreezing is calculated. In case of positive Q_0 or Q_1, the temperature is set to $0^{\circ}C$ and snowmelt m (m^3) is calculated using the equation

$$m = \frac{Q_m}{\rho h_f B}, \tag{13}$$

where Q_m is the energy available for melting (kJ), ρ is the density of water (kgm^-3), h_f is the latent heat of fusion (333.5 kJkg^-1) and B the fraction of ice in a unit mass of wet snow (Weber, 2013). After melting occurred in a time step, the snow cover thickness, snow density, liquid water content and relative saturation is adjusted.

3.1.4 Data requirements and interpolation

CRHM needs all meteorological input variables for each HRU. Therefore, the data from the DWD station (see section 2.3) needs to be interpolated for each HRU separately. The interpolation was done using the interpolation methods proposed by Liston and Elder (2006). Liston and Elder describe methods for temperature, relative humidity, wind speed, short-wave radiation, long-wave radiation and precipitation. Only long-wave radiation was calculated for each HRU using the method described in 2.3.2, which was specifically optimized for the Zugspitze catchment. The method for calculating short wave radiation was already described in detail in section 2.3.1. It is dependent on the aspect and therefore the variable which will be most influenced by changed aspect in a catchment. For details about the other methods, refer to Liston and Elder (2006).

3.2 HRU delineation

Considering the aim of this study, it was deemed necessary to make the HRU delineation as objective as possible. This would decrease variability of the results due to user specific choices. Furthermore, it would enable researchers to investigate more than one catchment, without losing comparability of their results. Especially for the investigation proposed in the outlook (see section 5), this would be desirable. The typical applied method for HRU delineation, using GIS-overlay procedures (Flügel et al., 1993), is largely dependent on subjective choices by the user. The here presented method, reduces the subjective choices and makes the chosen HRU dependent on the catchment characteristics and natural snow patterns.

Cluster Analysis was used to delineate the HRUs on basis of topographical and vegetational characteristics. In a parallel, study Weber et al. (2018) applied principal component

analysis (PCA) on the snow depths of the Zugspitze catchment from June 2014 to July 2017. The resulting natural patterns in the snow depth where used to compare the patterns of the cluster analysis and choose the most adequate number of clusters.

3.2.1 Data processing

For the cluster analysis, all catchment characteristics which should be used for delineation, have to be given in a raster format for the whole catchment. Two of the characteristics were already available: the elevation in form of a digital elevation model (DEM) with a 5m grid and the vegetation on a 2.5 m grid. The vegetation data consists of 4 categories: Forest, krummholz, grass and bedrock. To make it compatible, the vegetation data was aggregated to a 5 m raster. Both elevation and vegetation can be seen in figure 12a and 12b).

Additional topographic parameters were calculated using the information from the DEM. They were: slope, aspect and a wind sheltering index Sx. The following sections will describe these in detail.

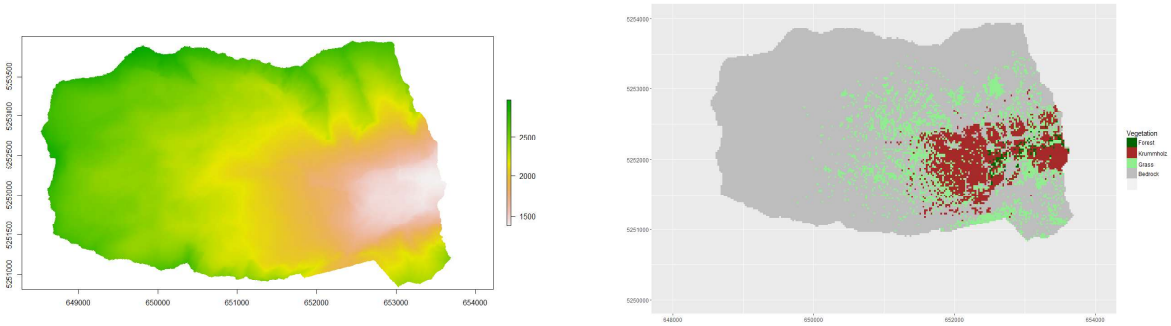

(a) (b)

Figure 12: Input Data: a) 5m Digital Elevation Model, b) Vegetation data

3.2.1.1 Slope and aspect

Slope and aspect were calculated using the *terrain* function of the R package *Raster*, using an algorithm by Fleming and Hoffer (1979) and Ritter (1987).

3.2.1.2 Sheltering index Sx

The mean sheltering index Sx (Winstral et al. 2002) was calculated for every cell of the raster and is the mean slope of the area in wind direction of the pixel. The 100 m search

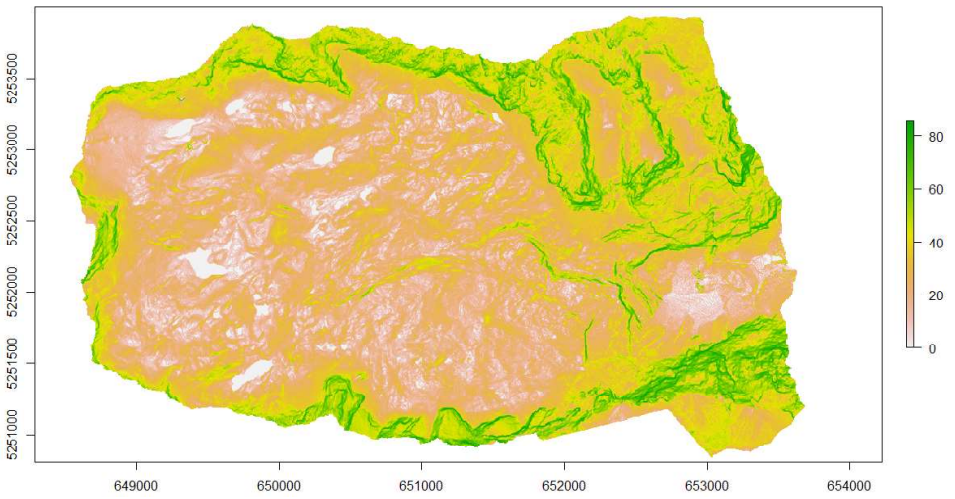

(a)

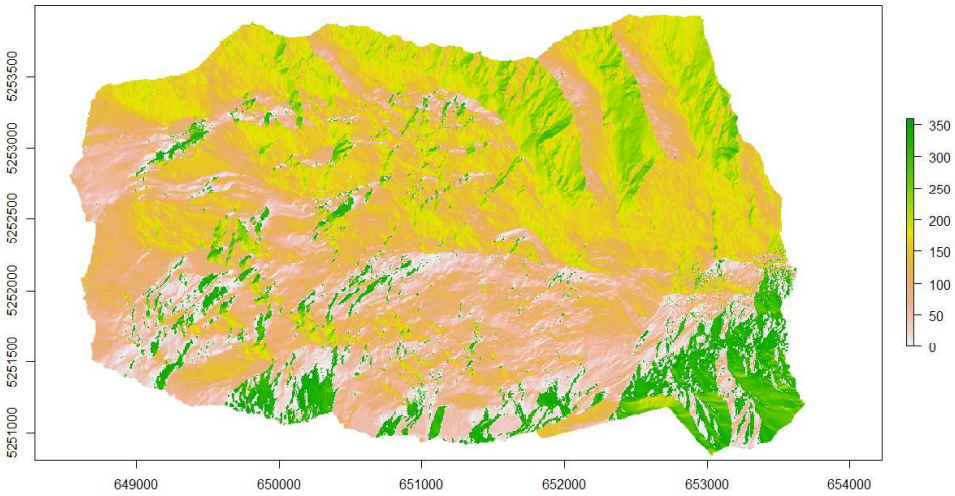

(b)

Figure 13: Topographic parameters of the Zugspitze:a) slope, b) aspect

vectors are "drawn" in a 30° angle in the main wind direction every 5 degrees, resulting in 7 transects. For each search vector, the overlaying raster cells are used to calculate the maximum slope for the transect:

$$Sx_{A,dmax}(x_i, y_i) = max\left[tan^{-1}\left(\frac{ELEV(x_v,y_v)-ELEV(x_i,y_i))}{[(x_v-x_i)]^2+(y_v-y_i)^2]^{0.5}}\right)\right], \tag{14}$$

where A is the azimuth of the search direction, (x_i, y_i) are the coordinates of the cell

of interest and (x_v, y_v) are the set of all cell coordinates located along the search vector (Winstral et al. 2002). The mean sheltering index Sx is then calculated by taking the mean maximum slope of all transects

$$\overline{Sx}_{dmax}(x_i, y_i) \,|_{A_1}^{A_2} = \frac{1}{n_v} \sum_{A=A_1}^{A_2} Sx_{A,dmax}(x_i, y_i), \tag{15}$$

where n_v is the number of search vectors defined by the search window A_1, A_2 and the search distance dmax.

The algorithm for calculating the mean sheltering index was written in R. The interpretation is the following: If the values are negative, then the area is not sheltered at all, leading to increasing wind speeds, while increasing positive values correspond to greater degrees of shelter due to more landscape obstacles.

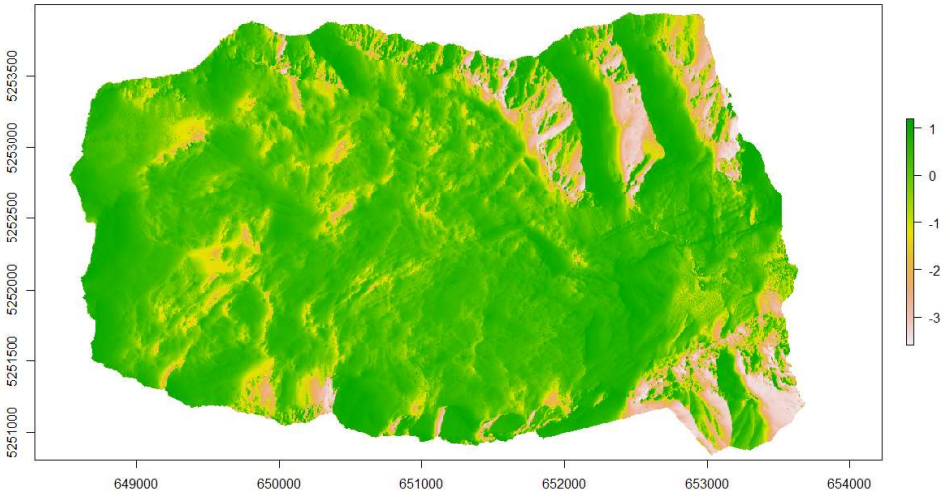

Figure 14: Mean sheltering index

3.2.2 Clustering algorithm

There is a large variety of cluster algorithms, for which it is crucial to calculate a distance matrix, e.g. hierarchical clustering methods, . This is not feasible in large data sets, such as the one which is used in this investigation: 1065480 raster cells produce a 1065480 × 1065480 matrix which would need approximately 100 GB ram to process. Therefore, the methods applicable for the used data are optimization algorithms, which partition the the n individuals (raster points) into the required number of groups. Furthermore, a method which can handle numerical and categorical data was needed, as the vegetational data is given as such.

Consequently. the *k-prototypes* Algorithm (Huang, 1998), a modification of the k-means algorithm for large mixed type data sets, was used for the HRU delineation. The basic principle behind *k-prototypes* is the same as in *kmeans*: The distances of points in a cluster to the cluster center, is minimized. In *kmeans*, the cluster center is the mean point of a certain cluster. In *k-prototypes* on the other hand, a cluster prototype is used as a cluster center. Because the objects are clustered against k prototypes, the algorithm is called *k-prototypes* algorithm.

The *k-prototypes* algorithm (Huang, 1998) divides the objects $X = X_1, X_2, ..., X_n$ into k disjunct groups, with k being a positive integer. Each element of X is represented by m attributes: $X_i = [x_{i1}, x_{i2}, ..., x_{im}]$. Instead of trying all possible combinations, a cost function is minimized to find the most adequate partition. The used cost function E in *k-prototypes* is

$$E = \sum_{l=1}^{k} \sum_{i=1}^{n} y_{il} d(X_i, Q_l), \tag{16}$$

with $Q_l = [q_{l1}, q_{l2}, ..., q_{lm}]$ the prototype vector for the cluster l, y_{il} an element of the partition matrix $Y_{n \times l}$ and d the similarity (or distance) measure. The partition matrix only contains the values of the set $\{0, 1\}$. $y_{il} = 1$ indicates that the object i is part of cluster l. In case of $y_{il} = 0$, object i is not part of cluster l.

The total cost of assigning X to the cluster l, is given by the inner part of equation 16: $E_l = \sum_{i=1}^{n} y_{il} d(X_i, Q_l)$. This is the sum of distances of objects inside cluster l and the cluster prototype. Often, the squared euclidean distance is used as a similarity measure (Huang, 1998). In case of a mixture of numerical and categorical values the distance (similarity

measure) for object i and prototype of cluster l is given as

$$d(X_i, Q_l) = \sum_{j=1}^{m_r} (x_{ij}^r - q_{ij}^r)^2 + \gamma_l \sum_{j=1}^{m_c} \delta(x_{ij}^c, q_{ij}^c), \tag{17}$$

with x_{ij}^r and Qij^r the numerical attributes, x_{ij}^c and Qij^c the categorical attributes and m_r and m_c the number of numerical and categorical attributes, respectively. The function δ is defined as

$$\delta(p, q) = \begin{cases} 0 & \text{if } p = q \\ 1 & \text{if } p \neq q \end{cases} \tag{18}$$

and γ_l is a weight for the categorical attributes. This weight defines the importance of the categorical value on the clustering. In case of $\gamma_l = 0$, the clustering only depends on the numerical variables and is equal to a k-means algorithm. If $\gamma_l > 0$, the clustering will be influenced by the categorical values, where larger values lead to more influence on the clustering results. The same γ value is used for all l cluster, hence $\gamma_l = \gamma \ \forall \ l \in k$. γ is calculated using the estimated average variance σ^2 of the numerical attributes. More precisely, kprototypes chooses γ as the mean σ^2, divided by 1 minus the sum of the squared relative frequencies of the categorical attributes.

Using the definition in equation 17, the total cost E_l of cluster l can be rewritten as

$$E_l = E_l^r + E_l^c, \tag{19}$$

with $E_l^r = \sum_{i=1}^{n} y_{il} \sum_{j=1}^{m_r} (x_{ij}^r - q_{ij}^r)^2$ and $E_l^c = \gamma \sum_{i=1}^{n} y_{il} \sum_{j=1}^{m_c} \delta(x_{ij}^c, q_{ij}^c)$. Therefore, the total cost is the sum of the total cost of all numerical attributes E_l^r and all categorical attributes E_l^c. This leads to the total cost of

$$E = \sum_{l=1}^{k} E_l^r + \sum_{l=1}^{k} E_l^c = E^r + E^c. \tag{20}$$

E can be minimized by minimizing both E^r and E^c (Huang, 1998).

The numerical part of the cost function E_r is minimized if the numerical entries of all k prototype vectors are equal to the mean of the object values in the corresponding k clusters. The cost of the categorical attributes is minimized, if the probability that a certain attribute is present in the cluster is larger or equal than in all the other clusters.

The *k-prototypes* algorithm is an iterative algorithm, which consists of 4 steps that are repeated until convergence. These 3 steps are:

1. Randomly choose k initial prototypes from the data set.
2. Assign each object to the nearest prototype according to equation 17 and then update the prototype of each region.
3. Reallocate the objects to the new prototypes

Those steps are repeated until a full cycle, where no object changes cluster.

3.2.3 Clustering

All numerical input variables are standardized by subtraction of the mean and dividing with the standard deviation. This is necessary for making the euclidean distance of all numerical variables comparable. The two glaciers in the Catchment have not been included in the clustering and were instead assigned to an additional HRU.

The chosen cluster algorithm is dependent on its randomly chosen initial cluster prototypes. Consequently the clustering, was repeated 100 times and the result, which minimizes the sum of distances, was chosen. This was done for all numbers of clusters which were deemed practical for further modeling applications: 2 to 14 clusters.

The Clustering results for the number of clusters from 7 to 10 are shown in figures 15a,15b, 15cand 15d.

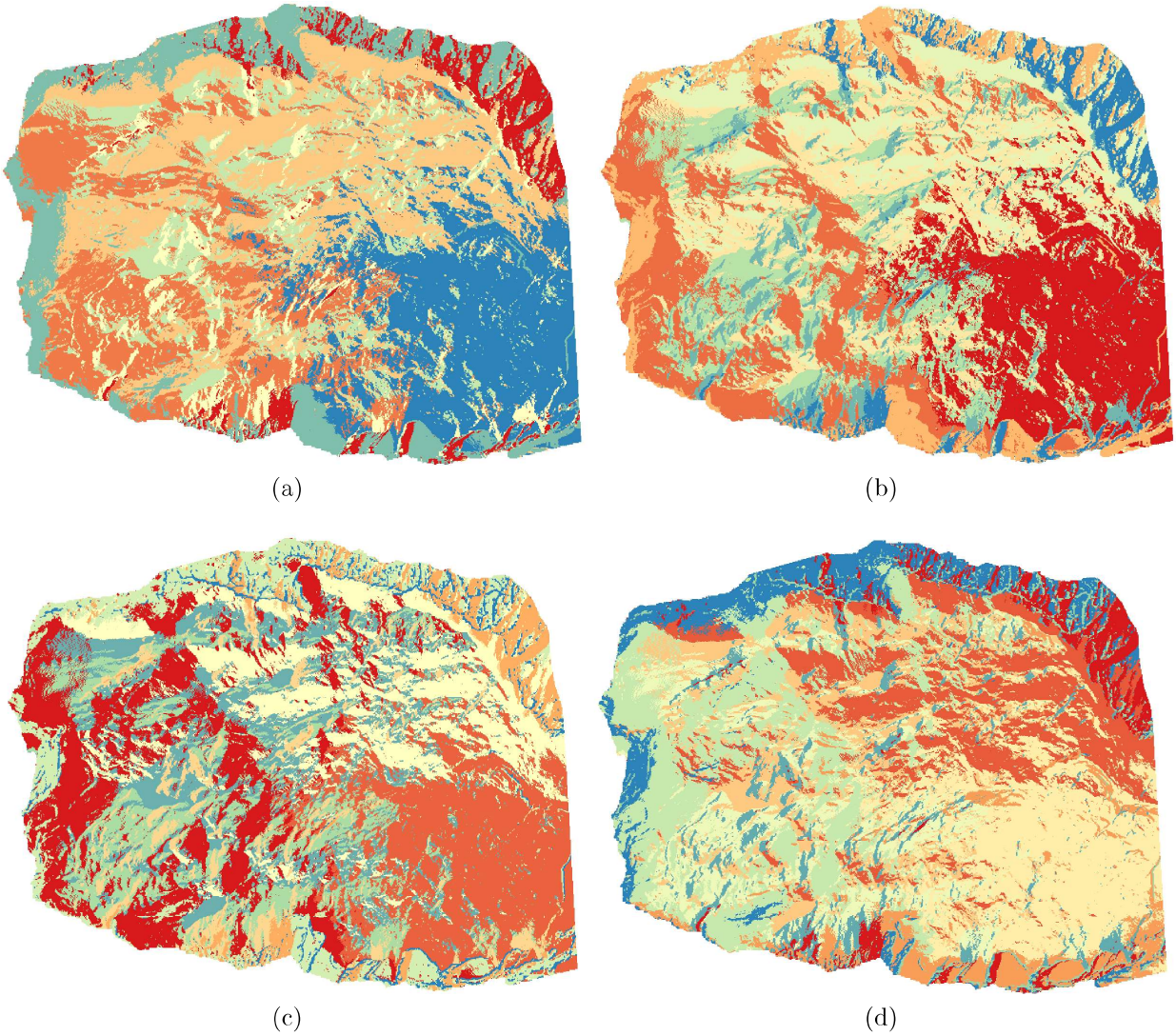

(a) (b)

(c) (d)

Figure 15: Resulting HRUs with a) 7 cluster, b) 8 cluster, c) 9 cluster, 10 cluster

3.2.4 Cluster validation with natural snow cover patterns

In the next step, the most adequate number of clusters had to be chosen for representing the catchment. This disadvantage of optimization algorithms leads to a subjective choice, which contradicts the aim of an objective method for HRU delineation. To avoid this, a comparison of the cluster results with natural snow patterns found in the 1. principal component (PC) of the accumulation period was used. The result of the cluster analysis which best represent those patterns is chosen. This comparison resulted in choosing the cluster result with 10 HRUs (9 cluster plus one glacier HRU). Figure 16 depicts the comparison of the clustering with 10 HRUs and the 1. PC of the accumulation period.

The cluster results, clearly reproduces the small scale patterns, especially in the western

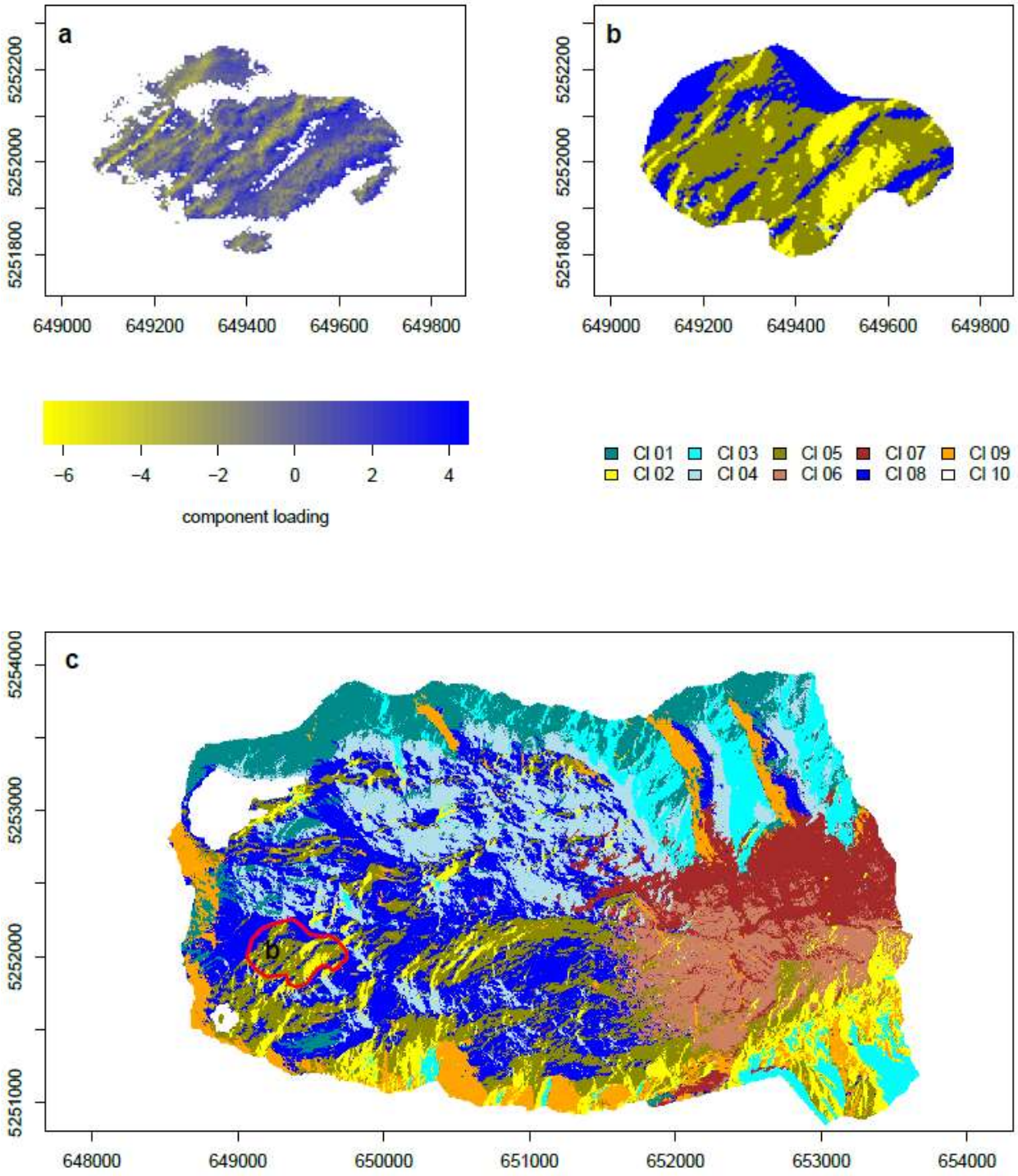

Figure 16: a) clustering result with 10 HRUs, b) HRUs in PCA covered area

part. Larger scale patterns in the eastern part are reproduced sufficiently. Furthermore, the dark blue cluster in figure 16 (cluster 8) fits the missing values in between and in the outline of the PCA. These missing values occur in south exposed parts of deeper troughs and are produced by shadowing effects during LIDAR measurements.

3.2.5 Chosen HRUs and rotated catchments

Figure 17 shows the result of the clustering with 10 cluster. The 10th HRU (in white) represents the two glaciers of the Zugspitze catchment and was not included in the clustering. The resulting HRUs can be characterized as follows:

- HRU 1: high elevation, steep northern hillsides, facing south
- HRU 2: high elevation, steep southern hillsides, facing north-east
- HRU 3: high elevation, steep hillsides, facing west
- HRU 4: medium elevation, not so steep, facing south-west
- HRU 5: medium elevation, not so steep, facing north
- HRU 6: low elevation, vegetated area
- HRU 7: low elevation, no vegetation, facing south
- HRU 8: medium elevation, not so steep, facing south
- HRU 9: high elevation, step hillsides, facing east
- HRU 10: Glaciers

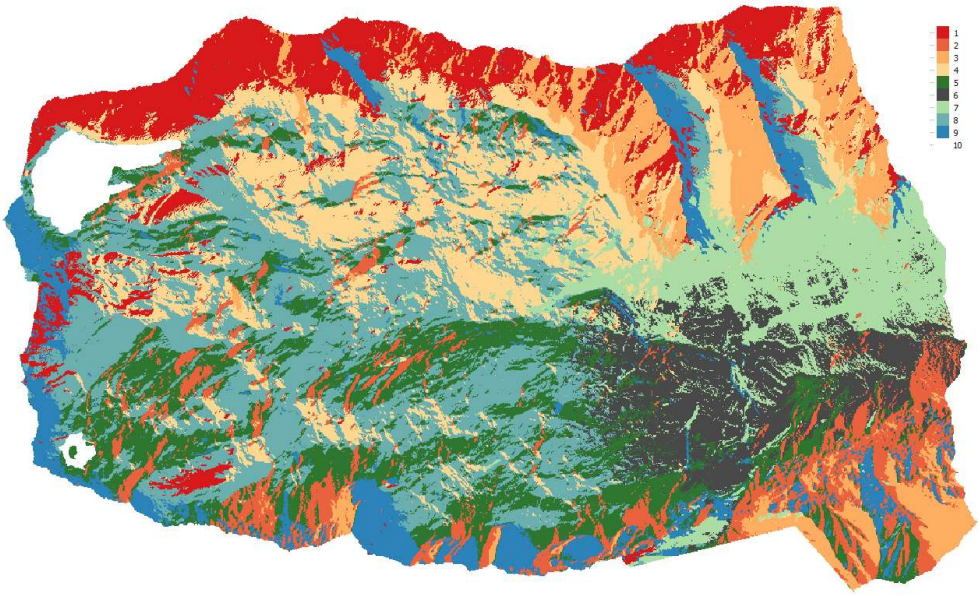

Figure 17: Chosen clustering result with 10 HRUs

The HRU specific parameter that are used in CRHM are given in Table 1. When rotating the catchment by 90°, 180°and 270°, only the aspect of the HRU is changed. To simulate the

Table 1: HRU parameters

HRU/cluster	elevation (m a.s.l.)	aspect (°)	slope (°)	land cover	area (km^2)
1	2598.02	161.33	44.35	rock	1.3
2	2103.72	329.41	36.38	rock	0.96
3	2311.64	244.52	45.95	rock	0.97
4	2321.48	175.94	24.00	rock	1.81
5	2228.46	29.33	21.76	rock	1.71
6	1686.75	82.13	25.97	knee wood	1.03
7	1802.82	156.22	40.08	knee wood	1.11
8	2329.34	102.79	19.26	rock	2.71
9	2376.03	59.91	50.53	rock	0.9
10	2614.56	81.1	14.45	ice	0.23

rotation of the catchment, the aspect of each raster cell of the catchment was changed and the resulting values averaged for each HRU. This produces new HRU specific aspect values for the rotated catchments. Those can be seen in table 2.

Table 2: Aspect (°) of rotated catchments

Zugspitze 90°	Zugspitze 180°	Zugspitze 270°
251.33	273.26	71.33
79.38	149.41	239.41
242.00	70.70	154.53
265.94	257.15	85.94
119.33	209.33	299.33
172.13	261.17	229.63
246.22	297.93	72.97
192.79	282.79	182.50
149.91	239.91	269.82
168.20	257.34	271.75

3.3 Analysis tool

To automatize the modelling of the catchments and the analysis of the resulting model outputs, an app was developed in the R package *shiny* (Chang et al., 2017). This app has two main functionalities:

1. Hydrological modelling of one of the four Zugspitze catchments with CRHM, which includes:
   (a) Modifying the WETTREG temperature data for a chosen trend
   (b) Interpolating the WETTREG data to all HRUs with the method described in section 3.3.1.
   (c) Creating an observation file with a corresponding CRHM project file and starting CRHM modelling
2. Analyzing the model outputs for a certain chosen trend for all 4 catchments for the time periods 1980-2015 and 2070-2100:
   (a) peak SWE (mm): catchment and time specific summary tables and interactive graphs
   (b) accumulated melt rate (mm/yr): catchment and time specific summary tables and interactive graphs
   (c) snow cover duration (days): catchment and time specific summary tables and interactive graphs

The starting panel of the app can be seen in figure 18. The next two sections will describe the functionality and the underlying methods in detail.

3.3.1 Hydrological modelling

Starting from the front panel, the user is able to choose a catchment for the following calculations, showing all the HRU parameters of the chosen catchment. After choosing a catchment the *Climate Change trend* panel is opened and a trend for the future time series can be chosen (see figure 19a). After selecting a new trend, the WETTREG temperature data set is shifted according to the chosen trend. This is done by fitting a simple two parameter

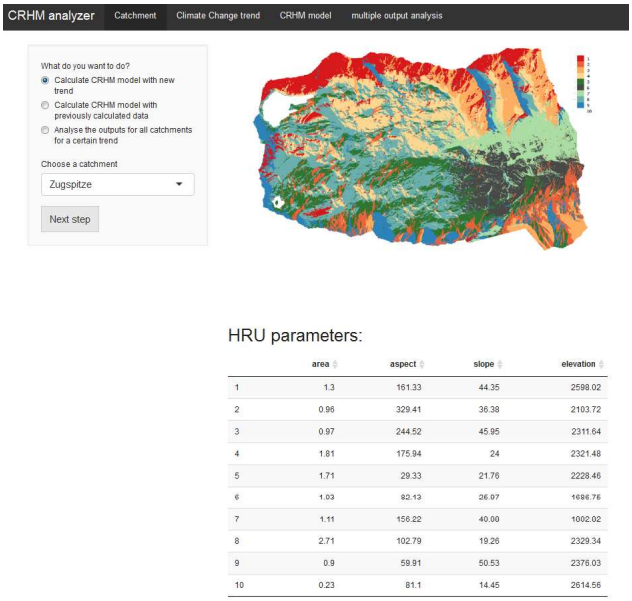

	area	aspect	slope	elevation
1	1.3	161.33	44.35	2598.02
2	0.96	329.41	36.38	2103.72
3	0.97	244.52	45.95	2311.64
4	1.81	175.94	24	2321.48
5	1.71	29.33	21.76	2228.46
6	1.03	82.13	26.07	1686.76
7	1.11	156.22	40.00	1002.02
8	2.71	102.79	19.26	2329.34
9	0.9	59.91	50.53	2376.03
10	0.23	81.1	14.45	2614.56

Figure 18: Analysis tool opening screen

linear model to temperature data and calculating for each time step the difference to a new trend with the same intercept, but with a different slope. This difference is then added to each time step, to induce the chosen trend on the existing data. The resulting time series is then plotted (see figure 19b).

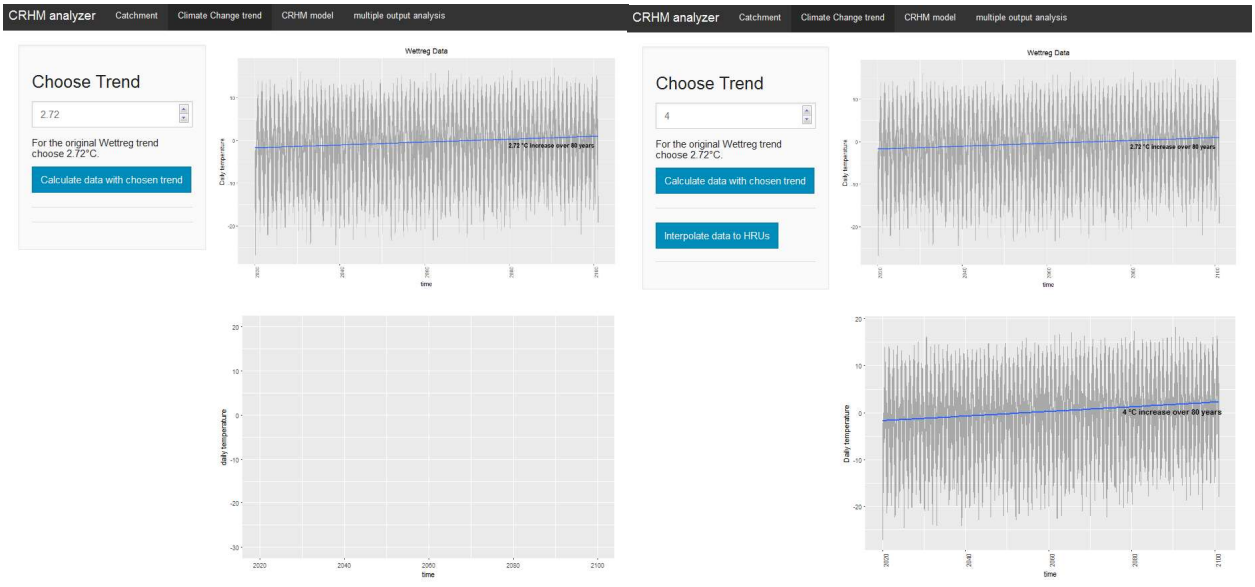

(a) (b)

Figure 19: Analysis tool - Choosing climate change trend

In the next step, the meteorological data from the DWD station is interpolated to each

HRU, as described in 3.1.4. This automatically creates a new CRHM input file, with all meteorological observations for all HRUs. After that, CRHM is started and the chosen catchment is modelled using the previously calculated input data. There is also an option where already prepared input data can be used to directly start CRHM. This option is available in the start panel (see figure 18). After modelling each of the 4 catchments with the same trend, the outputs can be analyzed in the second part of the app.

3.3.2 Analysis of multiple model outputs

The second main function of the app is an analysis tool. As input for this analysis, the CRHM outputs for all 4 catchments with a certain future temperature trend is needed. It uses the CRHM outputs SWE (mm), snowmeltD (snowmelt in mm/day) and z_s (total snow cover thickness in m) from the SnobalCRHM module (see section 3.1.3). In this analysis, three variables are calculated to compare and quantify the influence of climate change and changed aspect on the Zugspitze catchment. Those variables are the mean peak snow water equivalent (SWE), the accumulated melt rate and the snow cover duration. Those three variables are calculated and plotted for each of the 4 catchments for the past (1980-2015) and the future (2070-2100) time period. The analysis is separated into 5 different panels: "*peak SWE*", "*melt rate*", "*snow cover duration*", "*1980-2015*" and "*2070-2100*". Those panels and their underlying calculations will now be described in detail.

Peak SWE:

The mean peak SWE (mm) is the maximum SWE for a certain time period. It was calculated for the entire catchment for each season and for each HRU for every month. Both values were then averaged over the whole time period. Additionally, the changes from the past and the future time period are calculated. An example of the output can be seen in figure 20a. The outputs for the seasonal mean peak SWE for the catchments and the corresponding change are given in two tables. The HRU specific monthly mean peak SWE is given as an interactive plot. This plot can show the results of all HRUs (changable on the side panel) and show the values for each time step for all catchments. Additionally a map of the original Zugspitze catchment and its HRUs is given on the side panel, with information about the HRU number and mean elevation in m a.s.l..

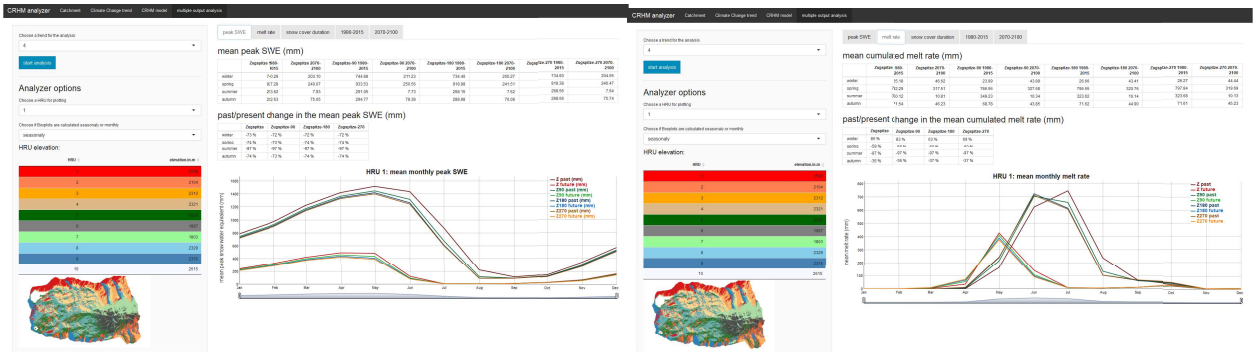

(a)

(b)

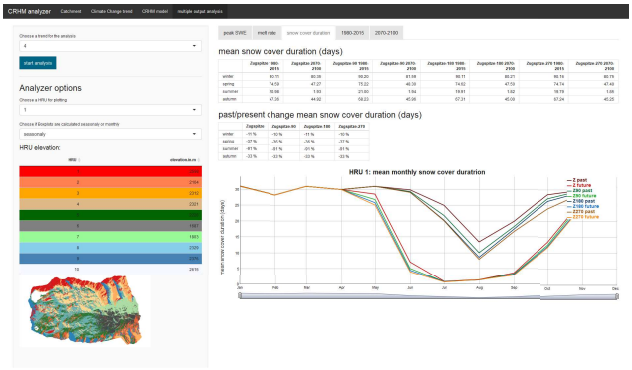

(c)

Figure 20: Tables and interactive plots for a) mean peak SWE, b) mean accumulated snow melt, c) mean snow cover duration

Melt rate:

The mean accumulated melt rate (mm) is the sum of melt rate per season and per month, averaged over all years for each catchment. Changes for past and future time period are calculated for each catchment and depicted with the seasonal results in two tables. The monthly results are given (as described above) as an interactive plot. See figure 20b for an output example.

Snow cover duration:

The snow cover duration is defined as the number of days with a snow cover > 5 cm (Wielke et al., 2004). Just as before, the values are aggregated seasonally and monthly and averaged over all years per catchment. An example of the resulting tables and the interactive plot can be seen in figure 20c.

1980-2015:

This panel includes only data from the past time period (1980-2015) for all 4 catchments. It contains tables and graphs for all three variables: mean peak SWE, mean accumulated

melt rate and mean snow cover duration. For all 3 variables and all catchments, a table with mean seasonal values is calculated. Furthermore, the main part of this panel, the boxplots of the 3 variables for either seasons or months is shown. This can be seen in figure 21a and figure 21b. The boxplots allow the comparison of the variable distributions..

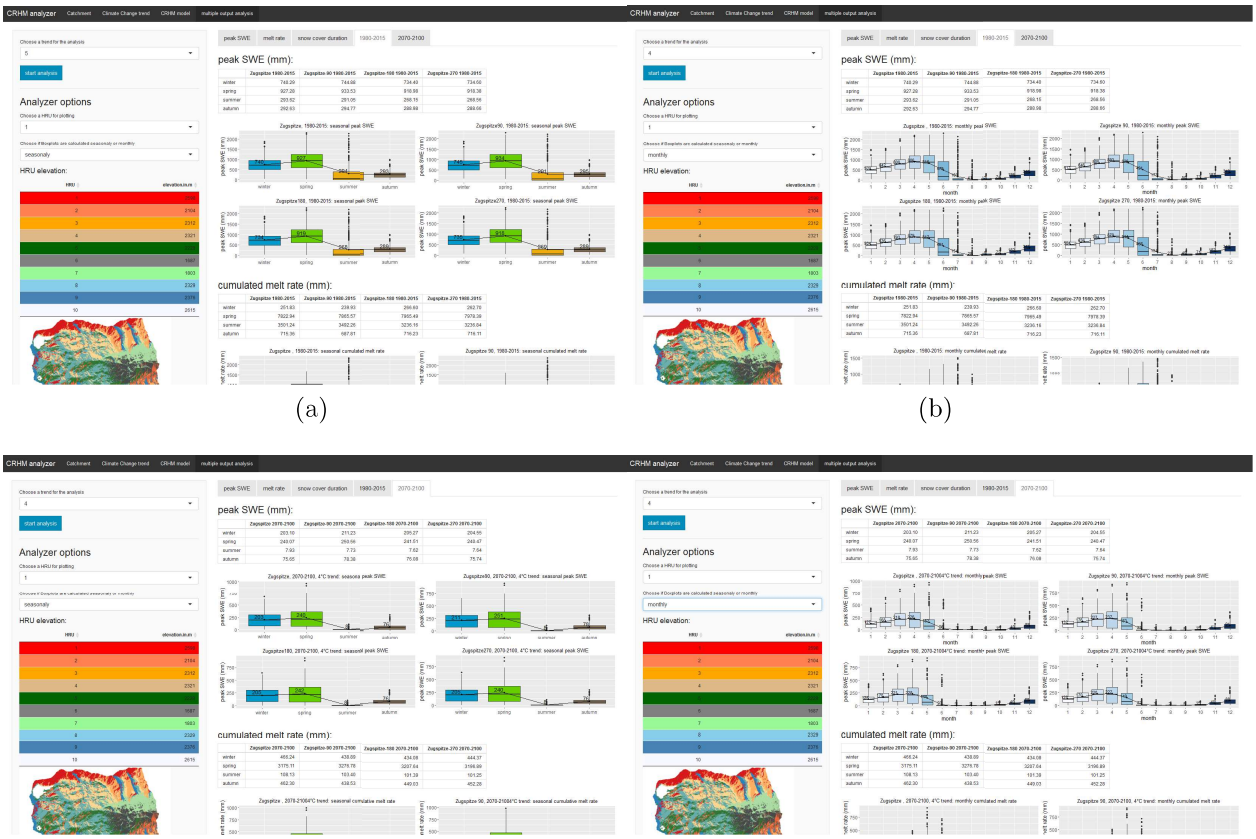

Figure 21: CRHM analysis a) 1980-2015 Panel seasonal plots, b) 1980-2015 Panel monthly plots, c) 2070-2100 Panel seasonal plots, d) 2070-2100 Panel monthly plots

2070-2100:

This panel contains the same information as the 1980-2015 panel, but for the future time period and with the chosen temperature trend. Examples can be seen in figure 21c and figure 21d.

The analysis function of the presented app makes the produced data easier comparable, more presentable and comes in handy for investigating the results in detail.

4 Results

4.1 Evaluation of HRU delination method

To evaluate the intersubjective delineating method, model outputs of snow depth are compared to measured snow depths of the DWD and LWD station. Additionally, the method is compared to a subjective delineation approach, which divides the Zugspitze catchments in 4 HRUs using the 4 vegetations Zones and the elevation, published by Weber et al. (2016). Figure 22a and 22b show the observed and with 10 HRUs modelled snow depth for the DWD and LWD station for the period 1998-2016. Comparing the modelled with the measured snow depth values results in an NSE (Nash and Sutcliffe, 1970) of 0.78 for the DWD station and 0.71 for the LWD station. Consequently, it can be stated, that CRHM produces reasonable results for accumulation and ablation processes at both stations.

To compare the 10 HRU ("best fit") model to models with the same clustering approach but different numbers of clusters (8, 12) and to the 4 HRU model by Weber et al. (2016), 3 snow indices were calculated in addition to the NSE values of the stations. The chosen snow indices were: yearly maximum snow water equivalent (MSWE)(mm), day of the maximum snow water equivalent (DoMSWE)(day of year) and the yearly snow cover duration (days). The resulting mean values for the entire catchment, weighted by HRU areas, are shown in table 3. From the efficiency values, it is clearly visible that the "best fit" model, which most adequately represents the dominant snow patterns, produces the best simulation results.

	MSWE (mm)	DoMSWE (day of year)	snow cover duration (days)	NSE (LWD)	NSE (DWD)
12 HRUs	681	113	234	0.65	0.70
10 HRUs ("best fit")	831	107	222	0.71	0.78
8 HRUs	651	113	233	0.61	0.68
4 HRUs	1039	121	257	0.68	0.35

Table 3: Snow indices and model efficiencies for models with different HRU numbers for clustering (12, 10, 8) and the 4 HRUs from Weber et al. (2016), for the years 1998-2016.

Examining the 4 HRU model by Weber et al. (2016), it can be observed that the snow cover of the highest HRU never melts completely and therefore a continuously growing snow pack is produced. This development was never observed in the catchment. The 10 HRU "best fit" model on the other hand produces a more realistic snow cover development, which

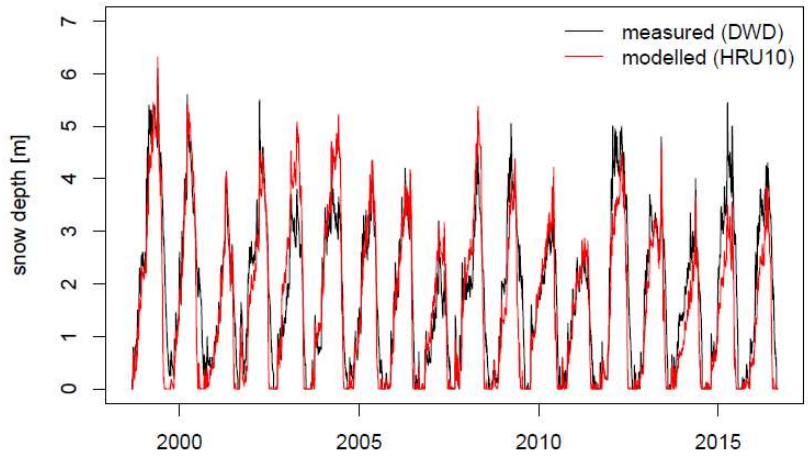

(a)

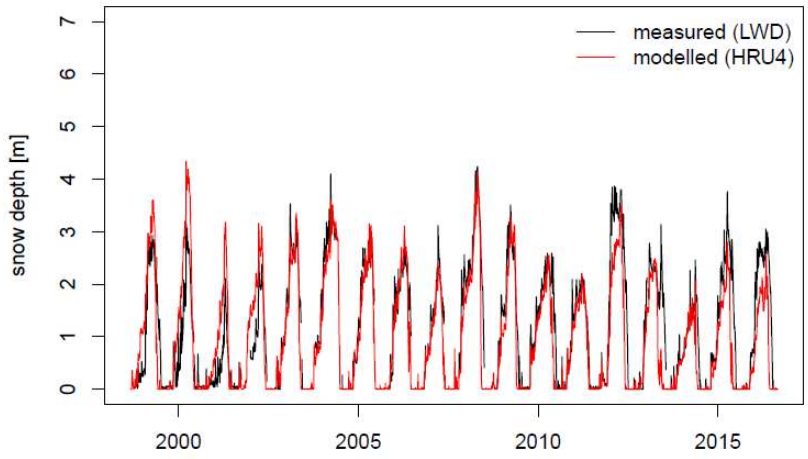

(b)

Figure 22: Comparing measured and with 10 HRU ("best fit") modelled snow depths results at the a) DWD station (NSE = 0.78), b) LWD station (NSE = 0.72)

can be seen in figure 23. This model shows that the HRU delineation scheme, using cluster HRUs fitted to natural snow patterns, seems to model snow ablation more appropriately.

To evaluate the influence of the number of HRUs on the model output, the three snow indices and the mean monthly runoff are examined. Comparing the different numbers of HRUs of the clustering delineation approach, a significantly wide range of values for the three snow indices is observed. Also, the range of values for the mean monthly runoff (averaged over 18 years) shows a wide range of calculated values, especially in the summer months. The range of values from the 8, 10 and 12 HRU model output is shown in figure 24. The black line shows the values from the "best fit" model. The "best fit" model has the lowest number of snow covered days and also the earliest day of the year with maximum

SWE. The maximum SWE has a big spread, with the "best fit" model approximately in the middle. The runoff shows a large variation in late spring and summer. These results provide clear evidence of a high variability of the modelled outputs, depending on the number of HRUs.

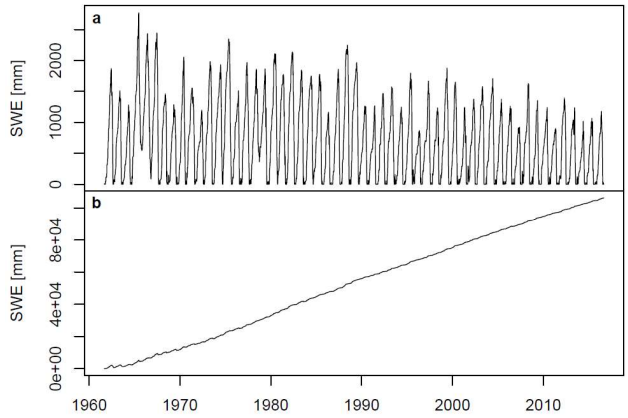

Figure 23: Snow cover results of highest HRU from a) 4 HRUs model by Weber et al. (2016), b) 10 HRU "best fit" model

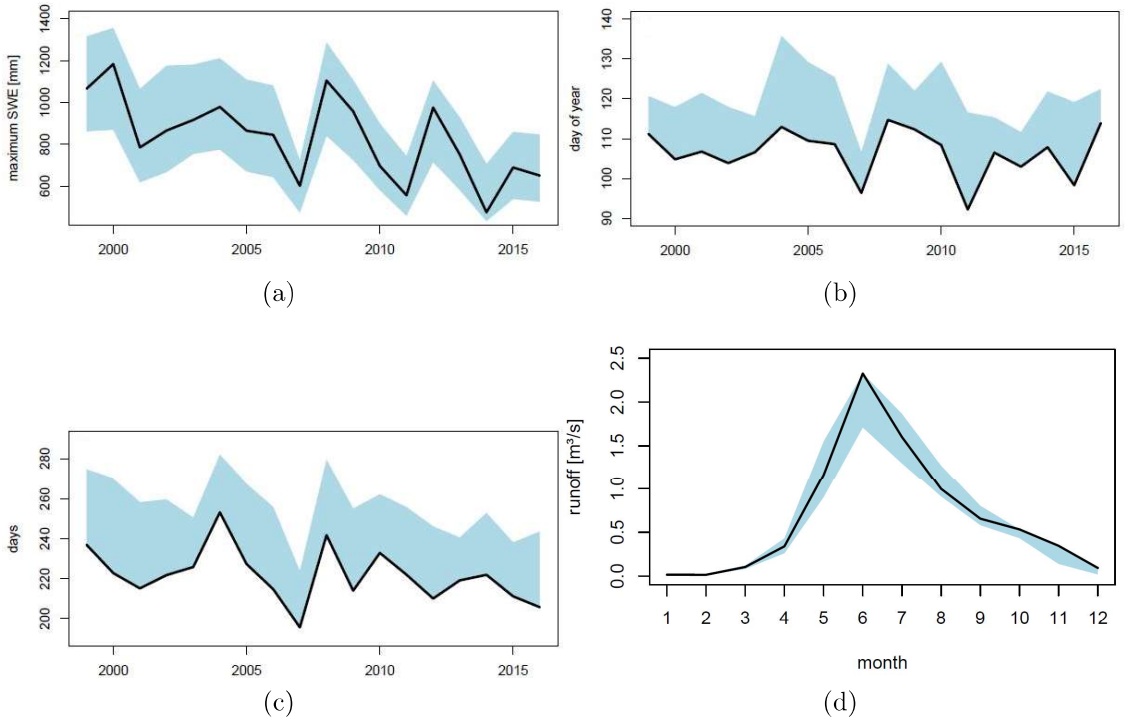

Figure 24: Range of values for the three snow indices and runoff for 8, 10 and 12 HRUs. a) Maximum snow water equivalent (MSWE) (mm), b) Day of MSWE (day of year), c) Snow cover duration (days) d) Mean monthly catchment runoff, averaged over 18 years. The bold black lines show the values of the 10 HRU "best fit" model.

4.2 Influence of aspect on climate change trend

In order to investigate the influence of changed aspect on climate change, the climate scenario with 3, 4 and 5° C was modelled and analyzed with the analysis tool (section 3.3.2). All values are given for the scenario with an 4°C increase, as it was observed that the resulting patterns are similar for all 3 scenarios and only differ in magnitude. For simplicity, the 4 catchments: Zugspitze, Zugspitze 90°, Zugspitze 180°, Zugspitze 270°, are called Z, Z90, Z180, Z270, respectively. For each of the three snow indices from the analysis tool first the seasonal aggregated values and then the monthly HRU specific values are examined.

4.2.1 Mean peak snow water equivalent

The seasonal average values did not change much due to the change in aspect. Therefore, the change from past to future stayed nearly the same for each catchment, with a 73% decrease in winter, a 74% decrease in spring, a 97% decrease in summer and a 74% decrease in autumn. The corresponding values are shown in table 4.

The mean monthly peak SWE showed a layering of the values, due to the influence of the changed aspect and therefore changed radiation balance (Figure 25). This layered structure is observable in both past and future time period, but differs in its spread. Peak SWE values from the past time period show a greater spread of values from March to May. In the climate change scenario this variability due to aspect change in the catchment is strongly reduced. With higher temperature increase this spread gets even narrower. This is apparent in figure 26, in which the results for HRU 7, for the climate change scenario with a 5° C increase, are shown.

Table 4: Mean peak SWE (mm), 4°C scenario

	Z 1980-2015	Z 2070-2100	Z 90 1980-2015	Z 90 2070-2100	Z 180 1980-2015	Z 180 2070-2100	Z 270 1980-2015	Z 270 2070-2100
winter	740.29	203.10	744.88	211.23	734.40	205.27	734.60	204.55
spring	927.28	240.07	933.53	250.56	918.98	241.51	918.38	240.47
summer	293.62	7.93	291.05	7.73	268.15	7.62	268.56	7.64
autumn	292.63	75.65	294.77	78.38	288.98	76.08	288.66	75.74

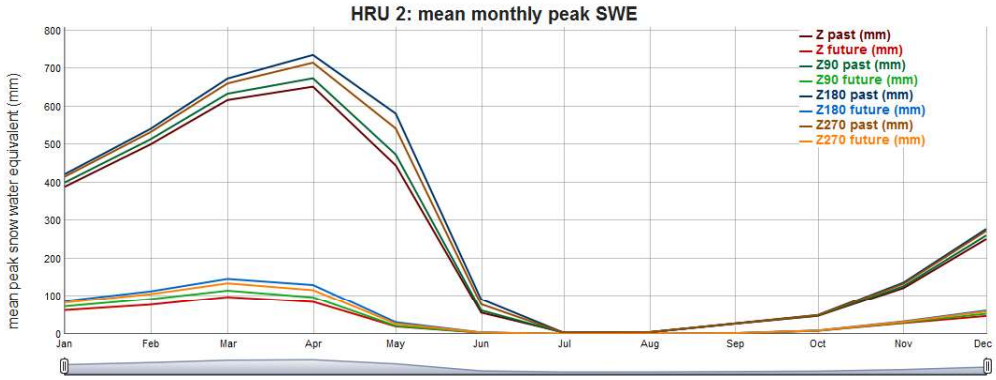

Figure 25: Mean monthly peak SWE for scenario with 4°C increase for HRU 2

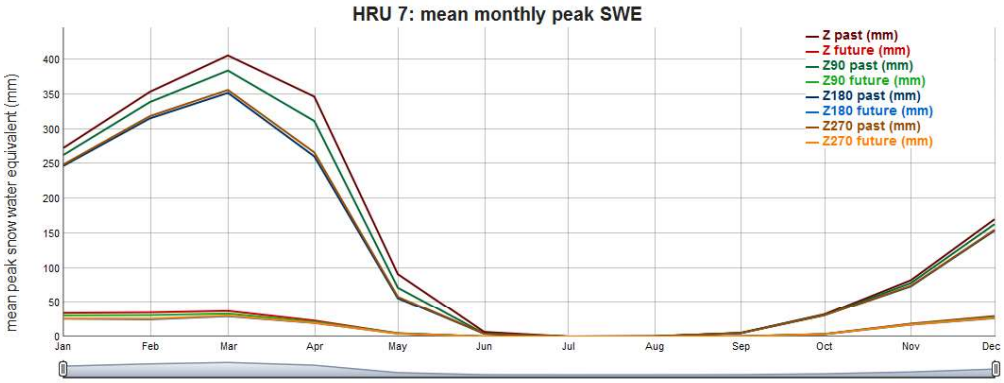

Figure 26: Mean monthly peak SWE for scenario with 5°C increase for HRU 7

4.2.2 Melt rate

The melt rate also does not show any significant changes in the seasonal accumulated values. The change in winter melt rate of the Z and Z 90 catchment is about 20% higher, but considering the low values in the winter melt rate, this difference is not large. The corresponding values can be seen in table 5.

In the monthly accumulated melt rate for each HRU, the same patterns as in the peak SWE can be observed. However in some HRUs there is a change in the month with the peak accumulated melt rate. Figure 27 shows two HRUs where the month with the highest runoff was shifted due to the aspect change. In figure 27a this is especially visible in the past time period but also in the future time period. Figure 27b shows an example where only the past time period is influenced by the change in the peak month, while the future time period stays unaffected. Figure 28 on the other hand shows the example of HRU 3, where only the future time period experiences a shift in the peak month. The shift in the month with peak accumulated melt rate in either past time period, future time period, or

both, is more visible in steep high altitude HRUs (1, 3, 9), but also in others (HRU 4 and 6). These HRUs experience different amounts of changes of monthly melt rates in each of the 4 catchments.

Table 5: Mean accumulated melt rate (mm), 4°C scenario

	Z 1980-2015	Z 2070-2100	Z 90 1980-2015	Z 90 2070-2100	Z 180 1980-2015	Z 180 2070-2100	Z 270 1980-2015	Z 270 2070-2100
winter	25.18	46.62	23.99	43.89	26.66	43.41	26.27	44.44
spring	782.29	317.51	786.56	327.68	796.55	320.76	797.84	319.69
summer	350.12	10.81	349.23	10.34	323.62	10.14	323.68	10.13
autumn	71.54	46.23	68.78	43.85	71.62	44.90	71.61	45.23

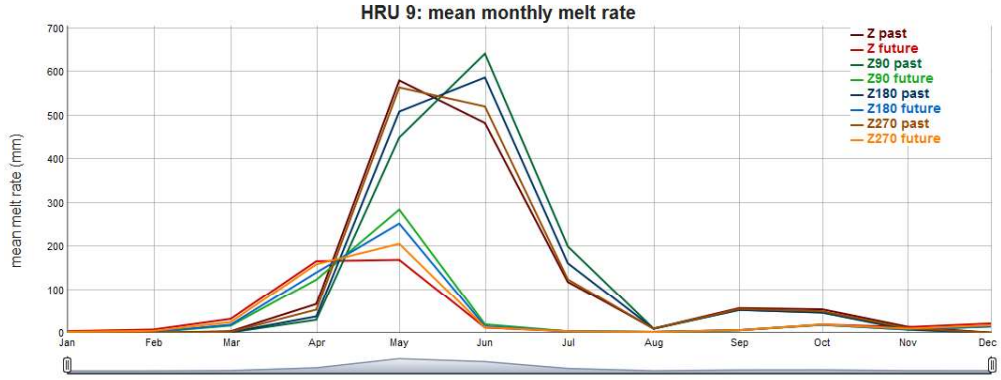

(a)

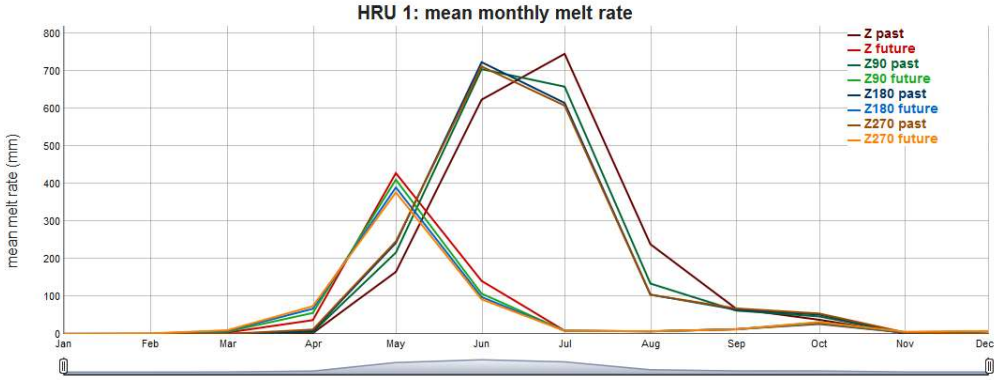

(b)

Figure 27: Monthly accumulated melt rate (mm) for 4°C scenario, with shifted peak due to aspect change, for a) HRU 9, b) HRU 1

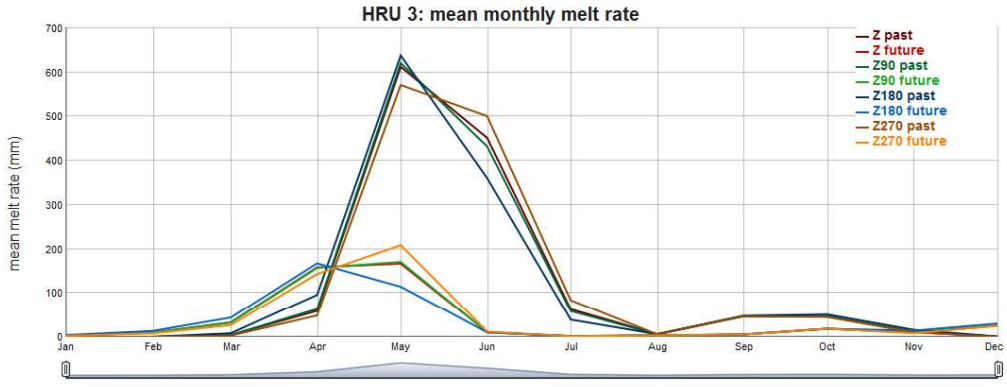

Figure 28: Monthly accumulated melt rate (mm) for 4°C scenario, with shifted peak due to aspect change, for HRU 3

4.2.3 Snow cover duration

Similar to the other two snow indices, the snow cover duration does not differ significantly for the seasonal aggregation for the whole catchments. The corresponding values can be seen in table 6. The monthly values show similar behaviour as for the two other indices. The same layering effect can be observed as before, but is hardly visible in flat HRUs. An example of the mean monthly snow cover duration for a steep HRU and for a flat HRU is given in figure 29a and figure 29b, respectively. Flat HRUs are hardly influenced by the different aspect of the 4 catchments, while steep HRUs show differences in the months May to October in both past and future time periods. The example in figure 29a shows an HRU were the 4 catchments will experience different reduction of the monthly snow cover duration in the months June to October.

Table 6: Mean snow cover duration (mm), 4°C scenario

	Z 1980-2015	Z 2070-2100	Z 90 1980-2015	Z 90 2070-2100	Z 180 1980-2015	Z 180 2070-2100	Z 270 1980-2015	Z 270 2070-2100
winter	90.11	80.35	90.20	81.59	90.11	80.21	90.16	80.75
spring	74.59	47.27	75.22	48.30	74.62	47.50	74.74	47.40
summer	20.98	1.93	21.00	1.94	19.91	1.82	19.79	1.85
autumn	67.36	44.92	68.23	45.96	67.31	45.00	67.24	45.25

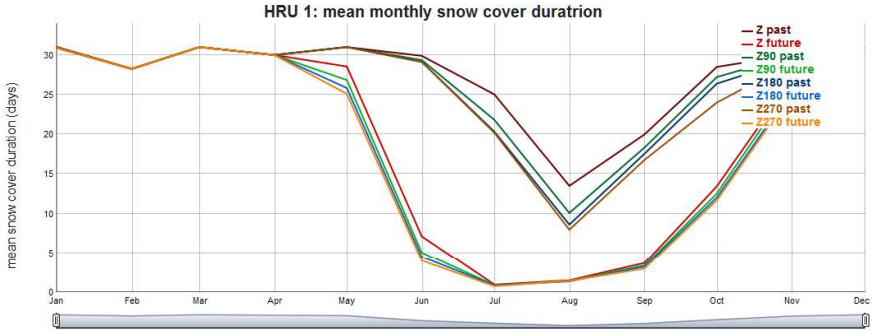

(a)

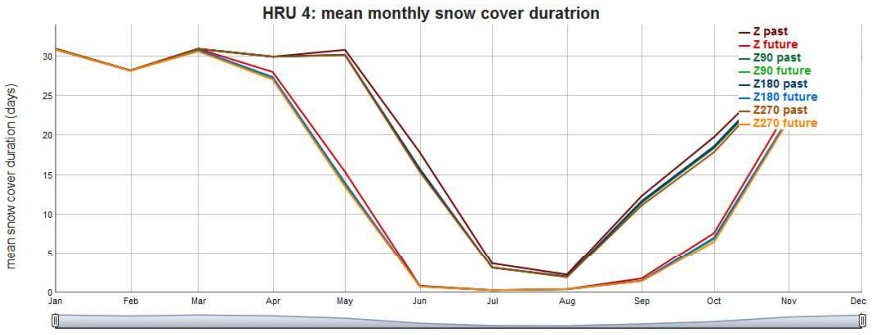

(b)

Figure 29: Mean monthly snow cover duration (mm) for 4°C scenario for a) a very steep HRU, b) a flat HRU

5 Discussion and outlook

To introduce a more objective way for HRU delineation, a clustering approach was combined with natural snow cover patterns derived with a principal component analysis (PCA). Before comparing it to other methods, it was shown that by using the resulting HRUs from this method, CRHM produces reasonably accurate results for accumulation and ablation processes at both hydroclimatological stations in the Zugspitze catchment. Comparing the results of this method with a subjective method using elevation and vegetational zones, the model efficiency is enhanced and the long term results show a better reflection of the catchment processes. It could also be shown that the number of HRUs chosen for the clustering approach has a strong influence on the model outputs. From these findings, it can be concluded that with the same delineation method, the number of HRUs is an important parameter, which can influence the simulated snow cover indices significantly. This leads to increased options for the User to influence the model outcomes, if no objective method is

applied. Thus, the intersubjective method for HRU delineation presented here has proven to produce the best results for modelling snow cover development.

The results show that a change in aspect only has a minor influence on peak SWE and snow cover duration. For seasonal averaged snow indices, this results in different absolute values, but nearly the same relative changes for catchments with different aspects. Examining the monthly averaged HRU-specific results, a clear layering of the calculated snow indices for the 4 catchments can be observed. The order of the layers seems to be associated with the changed aspect, but no clear pattern is visible. The layering is apparent in the observation and scenario period, but mostly does not influence the percentage change. As one would expect, steep high altitude HRUs (e.g. HRU 1, HRU 9) seem to be more influenced by the changed aspect. This results in different percentage changes in some months, due to the disappearance of the layering effect in the scenario period. Nevertheless, the influence is small compared to the overall range of values.

Both peak SWE and snow cover duration are associated with snow accumulation processes in the catchment. Therefore it can be stated that a change in aspect only minorly influences snow accumulation. This corresponds with findings in literature, which state that snow accumulation processes are mainly influenced by elevation and only partially by aspect (Jost et al., 2007).

In the monthly accumulated melt rate, an influence of the changed aspect is clearly visible. A shift in melt rate peaks by one month and a large difference (up to 160 mm) in the values for the 4 catchments is observed. These large monthly differences also emphasize the importance of using an energy-balance snow model instead of a Degree-Day model, where different aspects would produce no change in melt rates. These results correspond with the findings from previous studies, which state that snow melt, as opposed to snow accumulation, is influenced by aspect as much as elevation (Jost et al., 2007).

The results show that aspect possibly influences climate change impact on snow melt on a monthly aggregated level. It also implies that results from a climate change impact study in a catchment could give inaccurate estimates for adjacent catchments. This could have an influence on water management, as it can not only shift the peak melt rate, but also induce a large variability in the monthly accumulated melt rates (up to 160 mm).

To further investigate the influence of topography on the climate change impact on alpine

catchments, the methodology applied here should be extended to several catchments. The results could give insights on the influence of the combination of catchment characteristics. When using several catchments, it would be possible to use the same climatic input (observation and scenario) for multiple catchments and examine the different results. This could produce a more general statement about the sensitivity of climate change impact to catchment characteristics.

References

[Anderson et al., 1979] Anderson, E. A., Colbeck, S., Slaughter, C. W., Bissell, V., Male, D. H., Crook, A. G., and Wiesnet, D. R. (1979). Snow accumulation, distribution, melt, and runoff. *Eos, Transactions American Geophysical Union*, 60(21):465.

[Beniston et al., 2017] Beniston, M., Farinotti, D., Stoffel, M., Andreassen, L. M., Coppola, E., Eckert, N., Fantini, A., Giacona, F., Hauck, C., Huss, M., Huwald, H., Lehning, M., Lpez-Moreno, J.-I., Magnusson, J., Marty, C., Moran-Tejda, E., Morin, S., Naaim, M., Provenzale, A., Rabatel, A., Six, D., Sttter, J., Strasser, U., Terzago, S., and Vincent, C. (2017). The European mountain cryosphere: A review of past, current and future issues. *The Cryosphere Discussions*, pages 1–60.

[B.J. Garnier and Ohmura, 1970] B.J. Garnier and Ohmura, A. (1970). The evaluation of surface variations in solar radiation income. *Solar Energy*, 13:21–34.

[Blomenhofer et al., 2009] Blomenhofer, A., Gudera, T., Neumann, J., Schwebler, W., Sprenger, W., and Wingering, M. (2009). Auswirkungen des Klimawandels auf Bodenwasserhaushalt und Grundwasserneubildung in Baden-Wrttemberg, Bayern und Rheinland-Pfalz :Untersuchungen auf Grundlage von WETTREG2003- und WETTREG2006-Klimaszenarien; KLIWA-Projekt B 3.3.1 Simulation der Grundwasserneubildung mit regionalen Klimaszenarien.

[Brunt D., 1932] Brunt D. (1932). Notes on radiation in the atmosphere. I. *Quarterly Journal of the Royal Meteorological Society*, 58(247):389–420.

[Chang et al., 2017] Chang, W., Cheng, J., Allaire, J., Xie, Y., and McPherson, J. (2017). *shiny: Web Application Framework for R*. R package version 1.0.5.

[Clark, 1945] Clark, C. O. (1945). Storage and the Unit Hydrograph. *Proceedings of the American Society of Civil Engineers*, 69(9):1333–1360.

[Cordeiro et al., 2017] Cordeiro, M. R. C., Wilson, H. F., Vanrobaeys, J., Pomeroy, J. W., Fang, X., and Team, T. R.-A. P. B. M. (2017). Simulating cold-region hydrology in an intensively drained agricultural watershed in Manitoba, Canada, using the Cold Regions Hydrological Model. *Hydrology and Earth System Sciences; Katlenburg-Lindau*, 21(7):3483–3506.

[Davis et al., 1985] Davis, R. E., Dozier, J., LaChapelle, E. R., and Perla, R. (1985). Field and Laboratory Measurements of Snow Liquid Water by Dilution. *Water Resources Research*, 21(9):1415–1420.

[Dornes et al., 2008] Dornes, P. F., Pomeroy, J. W., Pietroniro, A., Carey, S. K., and Quinton, W. L. (2008). Influence of landscape aggregation in modelling snow-cover ablation and snowmelt runoff in a sub-arctic mountainous environment. *Hydrological Sciences Journal*, 53(4):725–740.

[Ellis et al., 2010] Ellis, C. R., Pomeroy, J. W., Brown, T., and MacDonald, J. (2010). Simulation of snow accumulation and melt in needleleaf forest environments. *Hydrol. Earth Syst. Sci.*, 14(6):925–940.

[Enke and Kreienkamp, 2006a] Enke, W. and Kreienkamp, F. (2006a). WETTREG A1b SCENARIO RUN, UBA PROJECT, 2061-2070. *http://cera-www.dkrz.de/WDCC/ui/Compact.jsp?acronym=WR_A1B_2061_2070*. type: dataset.

[Enke and Kreienkamp, 2006b] Enke, W. and Kreienkamp, F. (2006b). WETTREG A1b SCENARIO RUN, UBA PROJECT, 2071-2080. *http://cera-www.dkrz.de/WDCC/ui/Compact.jsp?acronym=WR_A1B_2071_2080*. type: dataset.

[Enke and Kreienkamp, 2006c] Enke, W. and Kreienkamp, F. (2006c). WETTREG A1b SCENARIO RUN, UBA PROJECT, 2081-2090. *http://cera-www.dkrz.de/WDCC/ui/Compact.jsp?acronym=WR_A1B_2081_2090*. type: dataset.

[Enke and Kreienkamp, 2006d] Enke, W. and Kreienkamp, F. (2006d). WETTREG A1b SCENARIO RUN, UBA PROJECT, 2091-2100. *http://cera-www.dkrz.de/WDCC/ui/Compact.jsp?acronym=WR_A1B_2091_2100*. type: dataset.

[Enke et al., 2005] Enke, W., Schneider, F., and Deutschlnder, T. (2005). A novel scheme to derive optimized circulation pattern classifications for downscaling and forecast purposes. *Theoretical and Applied Climatology*, 82(1-2):51–63.

[Essery Richard and Etchevers Pierre, 2004] Essery Richard and Etchevers Pierre (2004). Parameter sensitivity in simulations of snowmelt. *Journal of Geophysical Research: Atmospheres*, 109(D20).

[Etter et al., 2017] Etter, S., Addor, N., Huss, M., and Finger, D. (2017). Climate change impacts on future snow, ice and rain runoff in a Swiss mountain catchment using multi-dataset calibration. *Journal of Hydrology: Regional Studies*, 13(Supplement C):222–239.

[Fang and Pomeroy, 2008] Fang, X. and Pomeroy, J. W. (2008). Drought impacts on Canadian prairie wetland snow hydrology. *Hydrological Processes*, 22(15):2858–2873.

[Flgel, 1995] Flgel, W.-A. (1995). Delineating hydrological response units by geographical information system analyses for regional hydrological modelling using PRMS/MMS in the drainage basin of the River Brl, Germany. *Hydrological Processes*, 9(3-4):423–436.

[Friedmann and Korch,] Friedmann, A. and Korch, O. Die Vegetation des Zugspitzplatts (Wettersteingebirge, Bayerische Alpen): Aktueller Zustand und Dynamik. page 19.

[Granger and Pomeroy, 1997] Granger, R. J. and Pomeroy, J. W. (1997). Sustainability of the western Canadian boreal forest under changing hydrological conditions. II. Summer energy and water use. *Sustainability of Water Resources under Increasing Uncertainty, IAHS Publ. no. 240*, page 8.

[Gray et al., 2001] Gray, D. M., Toth, B., Zhao, L., Pomeroy, J. W., and Granger, R. J. (2001). Estimating areal snowmelt infiltration into frozen soils. *Hydrological Processes*, 15(16):3095–3111.

[Group, 2015] Group, M. R. I. E. W. (2015). Elevation-dependent warming in mountain regions of the world. *Nature Climate Change*, 5(5):424.

[Hagg,] Hagg, W. Bayerische Gletscher.

[Hagg et al., 2012] Hagg, W., Mayer, C., Mayr, E., and Heilig, A. (2012). Climate and glacier fluctuations in the Bavarian Alps during the past 120 years. *Erdkunde*, pages 121–142.

[Hinckley et al., 2012] Hinckley, E.-L. S., Ebel, B. A., Barnes, R. T., Anderson, R. S., Williams, M. W., and Anderson, S. P. (2012). Aspect control of water movement on hillslopes near the rain-snow transition of the Colorado Front Range: SNOWMELT AND HYDROLOGICAL FLOW PATHS ON OPPOSING HILLSLOPE ASPECTS. *Hydrological Processes*, 28(1):74–85.

[Huang, 1998] Huang, Z. (1998). Clustering large data sets with mixed numeric and categorical values. In *In The First Pacific-Asia Conference on Knowledge Discovery and Data Mining*, pages 21–34.

[Huss et al., 2017] Huss, M., Bookhagen, B., Huggel, C., Jacobsen, D., Bradley, R., Clague, J., Vuille, M., Buytaert, W., Cayan, D., Greenwood, G., Mark, B., Milner, A., Weingartner, R., and Winder, M. (2017). Toward mountains without permanent snow and ice. *Earth's Future*, 5(5):2016EF000514.

[IPCC, 2013] IPCC (2013). Summary for Policymakers. *Climate Change 2013: The Physical Science Basis. Contribution of Working Group I to the Fifth Assessment Report of the Intergovernmental Panel on Climate Chan*.

[Jost et al., 2007] Jost, G., Weiler, M., Gluns, D. R., and Alila, Y. (2007). The influence of forest and topography on snow accumulation and melt at the watershed-scale. *Journal of Hydrology*, 347(1-2):101–115.

[Klein et al., 2016] Klein, G., Vitasse, Y., Rixen, C., Marty, C., and Rebetez, M. (2016). Shorter snow cover duration since 1970 in the Swiss Alps due to earlier snowmelt more than to later snow onset. *Climatic Change*, 139(3-4):637–649.

[Klmt, 2005] Klmt, A. (2005). Langzeitverhalten der Lufttemperatur in Baden-Wrttemberg und Bayern: KLIWA-Projekt A 1.2.3 Analyse des Langzeitverhaltens von Gebietsmittelwerten der Lufttemperatur in Baden-Wrttemberg und Bayern.

[Klmt, 2008] Klmt, A. (2008). Langzeitverhalten von Sonnenscheindauer und Globalstrahlung sowie von Verdunstung und klimatischer Wasserbilanz in Baden-Wrttemberg und Bayern: KLIWA-Projekt A 1.2.1 /1.2.2 "Flchendeckende Analyse des Langzeitverhaltens der potentiellen und tatschlichen Verdunstungshhe", KLIWA-Projekt A 1.2.4 "Langzeitverhalten der Sonnenscheindauer und Globalstrahlung fr hydrologische Auswertungen".

[Kohler et al., 2014] Kohler, T., Wehrli, A., and Jurek, M., editors (2014). *Mountains and climate change: a global concern*. Sustainable mountain development series. Centre for Development and Environment [u.a.], Bern. OCLC: 900680198.

[Konzelmann et al., 1994] Konzelmann, T., van de Wal, R. S. W., Greuell, W., Bintanja, R., Henneken, E. A. C., and Abe-Ouchi, A. (1994). Parameterization of global and longwave incoming radiation for the Greenland Ice Sheet. *Global and Planetary Change*, 9(1):143–164.

[Krogh et al., 2017] Krogh, S. A., Pomeroy, J. W., and Marsh, P. (2017). Diagnosis of the hydrology of a small Arctic basin at the tundra-taiga transition using a physically based hydrological model. *Journal of Hydrology*, 550(Supplement C):685–703.

[Krogh et al., 2014] Krogh, S. A., Pomeroy, J. W., and McPhee, J. (2014). Physically Based Mountain Hydrological Modeling Using Reanalysis Data in Patagonia. *Journal of Hydrometeorology*, 16(1):172–193.

[Kunkel, 1989] Kunkel, K. E. (1989). Simple Procedures for Extrapolation of Humidity Variables in the Mountainous Western United States. *Journal of Climate*, 2(7):656–669.

[Kyle et al., 1985] Kyle, H. L., Ardanuy, P. E., and Hurley, E. J. (1985). The Status of the Nimbus-7 Earth-Radiation-Budget Data Set. *Bulletin of the American Meteorological Society*, 66(11):1378–1388.

[Knig-Langlo and Augstein, 1994] Knig-Langlo, G. and Augstein, E. (1994). Parameterization of the downward long-wave radiation at the Earth's surface in polar regions. *Meteorologische zeitschrift, N.F.3, Jg. 1994, H. 6*, pages 343–347.

[Leavesley et al., 1983] Leavesley, G., W. Lichty, R., M. Troutman, B., and G. Saindon, L. (1983). Precipitation-runoff modeling system (PRMS)User's Manual. *Water Resour. Invest. Rep*, 834238.

[Liston and Elder, 2006] Liston, G. E. and Elder, K. (2006). A Meteorological Distribution System for High-Resolution Terrestrial Modeling (MicroMet). *Journal of Hydrometeorology*, 7(2):217–234.

[Lopez-Moreno et al., 2013] Lopez-Moreno, J. I., Pomeroy, J. W., Revuelto, J., and Vicente-Serrano, S. M. (2013). Response of snow processes to climate change: spatial variability in a small basin in the Spanish Pyrenees. *Hydrological Processes*, 27(18):2637–2650.

[Lopez-Moreno et al., 2014] Lopez-Moreno, J. I., Revuelto, J., Gilaberte, M., Morn-Tejeda, E., Pons, M., Jover, E., Esteban, P., Garca, C., and Pomeroy, J. W. (2014). The effect of slope aspect on the response of snowpack to climate warming in the Pyrenees. *Theoretical and Applied Climatology*, 117(1-2):207–219.

[Mahmood et al., 2017] Mahmood, T. H., Pomeroy, J. W., Wheater, H. S., and Baulch, H. M. (2017). Hydrological responses to climatic variability in a cold agricultural region. *Hydrological Processes*, 31(4):854–870.

[Male and Granger, 1981] Male, D. H. and Granger, R. J. (1981). Snow surface energy exchange. *Water Resources Research*, 17(3):609–627.

[Marks et al., 1999] Marks, D., Domingo, J., Susong, D., Link, T., and Garen, D. (1999). A spatially distributed energy balance snowmelt model for application in mountain basins. *Hydrological Processes*, 13(12-13):1935–1959.

[Marks and Dozier, 1992] Marks, D. and Dozier, J. (1992). Climate and energy exchange at the snow surface in the Alpine Region of the Sierra Nevada: 2. Snow cover energy balance. *Water Resources Research*, 28(11):3043–3054.

[Marks et al., 1992] Marks, D., Dozier, J., and Davis, R. E. (1992). Climate and energy exchange at the snow surface in the Alpine Region of the Sierra Nevada: 1. Meteorological measurements and monitoring. *Water Resources Research*, 28(11):3029–3042.

[Marks et al., 1998] Marks, D., Kimball, J., Tingey, D., and Link, T. (1998). The sensitivity of snowmelt processes to climate conditions and forest cover during rain-on-snow: a case study of the 1996 Pacific Northwest flood. *Hydrological Processes*, 12(10-11):1569–1587.

[Miller, 1962] Miller, H. (1962). *Zur Geologie des westlichenWetterstein- und Mieminger Gebirges (Tirol). Strukturzusammenhnge am Ostrand des Ehrwalder Beckens.* PhD thesis, LMU Mnchen.

[Nash and Sutcliffe, 1970] Nash, J. E. and Sutcliffe, J. V. (1970). River flow forecasting through conceptual models part I A discussion of principles. *Journal of Hydrology*, 10(3):282–290.

[Neupane et al., 2017] Neupane, R. P., Adamowski, J. F., White, J. D., and Kumar, S. (2017). Future streamflow simulation in a snow-dominated Rocky Mountain headwater catchment. *Hydrology Research*, page nh2017024.

[Ohmura, 2001] Ohmura, A. (2001). Physical Basis for the Temperature-Based Melt-Index Method. *Journal of applied meteorology*, 40:9.

[Pomeroy and Li, 2000] Pomeroy, J. and Li, L. (2000). Prairie and arctic areal snow cover mass balance using a blowing snow model. *Journal of Geophysical Research: Atmospheres*, 105(D21):26619–26634.

[Pomeroy, 1989] Pomeroy, J. W. (1989). A Process-Based Model of Snow Drifting. *Annals of Glaciology*, 13:237–240.

[Pomeroy et al., 2007] Pomeroy, J. W., Gray, D. M., Brown, T., Hedstrom, N. R., Quinton, W. L., Granger, R. J., and Carey, S. K. (2007). The cold regions hydrological model: a platform for basing process representation and model structure on physical evidence. *Hydrological Processes*, 21(19):2650–2667.

[Rappl et al., 2010] Rappl, A., Wetzel, K.-F., Bttner, M., and Scholz, M. (2010). Tracerhydrologische Untersuchungen am Partnach-Ursprung | HyWa. *Hydrologie und Wasserbewirtschaftung*, 54. Jahrgang, Heft 4.

[Rasouli et al., 2014] Rasouli, K., Pomeroy, J. W., Janowicz, J. R., Carey, S. K., and Williams, T. J. (2014). Hydrological sensitivity of a northern mountain basin to climate change. *Hydrological Processes*, 28(14):4191–4208.

[Reich, 2005] Reich, T. (2005). Langzeitverhalten des Gebietsniederschlags in Baden-Wrttemberg und Bayern: KLIWA-Projekt A 1.1.1 "Bereitstellung von langen Reihen interpolierter Gitterpunktwerte des Niederschlags mit Hilfe des Verfahrens BONIE" und KLIWA-Projekt A 1.1.2 "Langzeituntersuchungen von Gebietswertreihen des Niederschlags".

[Rutter et al., 2009] Rutter, N., Essery, R., Pomeroy, J., Altimir, N., Andreadis, K., Baker, I., Barr, A., Bartlett, P., Boone, A., Deng, H., Douville, H., Dutra, E., Elder, K., Ellis, C., Feng, X., Gelfan, A., Goodbody, A., Gusev, Y., Gustafsson, D., Hellstrm, R., Hirabayashi, Y., Hirota, T., Jonas, T., Koren, V., Kuragina, A., Lettenmaier, D., Li, W.-P., Luce, C., Martin, E., Nasonova, O., Pumpanen, J., Pyles, R. D., Samuelsson, P., Sandells, M., Schdler, G., Shmakin, A., Smirnova, T. G., Sthli, M., Stckli, R., Strasser, U., Su, H., Suzuki, K., Takata, K., Tanaka, K., Thompson, E., Vesala, T., Viterbo, P., Wiltshire, A., Xia, K., Xue, Y., and Yamazaki, T. (2009). Evaluation of forest snow processes models (SnowMIP2). *Journal of Geophysical Research: Atmospheres*, 114(D6):D06111.

[Sedlar and Hock, 2009] Sedlar, J. and Hock, R. (2009). Testing longwave radiation parameterizations under clear and overcast skies at Storglaciren, Sweden. *The Cryosphere*, 3(1):75–84.

[Serquet et al., 2011] Serquet, G., Marty, C., Dulex, J.-P., and Rebetez, M. (2011). Seasonal trends and temperature dependence of the snowfall/precipitation-day ratio in Switzerland: SNOWFALL/PRECIPITATION-DAY RATIO. *Geophysical Research Letters*, 38(7):n/a–n/a.

[Spekat et al., 2007] Spekat, A., Enke, W., and Kreienkamp, F. (2007). *Neuentwicklung von regional hoch aufgelsten Wetterlagen fr Deutschland und Bereitstellung regionaler Klimaszenarios auf der Basis von globalen Klimasimulationen mit dem Regionalisierungsmodell WETTREG*. Umweltbundesamt.

[Tolson and Shoemaker, 2007] Tolson, B. A. and Shoemaker, C. A. (2007). Dynamically dimensioned search algorithm for computationally efficient watershed model calibration. *Water Resources Research*, 43(1).

[Uhlmann et al., 2009] Uhlmann, B., Goyette, S., and Beniston, M. (2009). Sensitivity analysis of snow patterns in Swiss ski resorts to shifts in temperature, precipitation and humidity under conditions of climate change. *International Journal of Climatology*, 29(8):1048–1055.

[Verseghy Diana L., 1991] Verseghy Diana L. (1991). ClassA Canadian land surface scheme for GCMS. I. Soil model. *International Journal of Climatology*, 11(2):111–133.

[Viviroli et al., 2011] Viviroli, D., Archer, D. R., Buytaert, W., Fowler, H. J., Greenwood, G. B., Hamlet, A. F., Huang, Y., Koboltschnig, G., Litaor, M. I., Lpez-Moreno, J. I., Lorentz, S., Schdler, B., Schreier, H., Schwaiger, K., Vuille, M., and Woods, R. (2011). Climate change and mountain water resources: overview and recommendations for research, management and policy. *Hydrology and Earth System Sciences; Katlenburg-Lindau*, 15(2).

[Viviroli et al., 2007] Viviroli, D., Drr, H. H., Messerli, B., Meybeck, M., and Weingartner, R. (2007). Mountains of the world, water towers for humanity: Typology, mapping, and global significance. *Water Resources Research*, 43(7):W07447.

[Viviroli and Weingartner, 2004] Viviroli, D. and Weingartner, R. (2004). The hydrological significance of mountains: from regional to global scale. *Hydrology and Earth System Sciences Discussions*, 8(6):1017–1030.

[Weber et al., 2018] Weber, M., Bernhardt, M., and Feigl, M. (2018). On the Ability of LIDAR Snow Depth Measurements to Determine or Evaluate the HRU Discretization in a Land Surface Model, Manuscript in preparation.

[Weber et al., 2016] Weber, M., Bernhardt, M., Pomeroy, J. W., Fang, X., Hrer, S., and Schulz, K. (2016). Description of current and future snow processes in a small basin in the Bavarian Alps. *Environmental Earth Sciences*, 75(17):1223.

[Wielke et al., 2004] Wielke, L.-M., Haimberger, L., and Hantel, M. (2004). Snow cover duration in Switzerland compared to Austria. *Meteorologische Zeitschrift*, 13(1):13–17.

[Winstral et al., 2002] Winstral, A., Elder, K., and Davis, R. E. (2002). Spatial Snow Modeling of Wind-Redistributed Snow Using Terrain-Based Parameters. *Journal of Hydrometeorology*, 3(5):524–538.

[WMO, 2011] WMO (2011). *Technical regulations: basic documents no. 2*. World Meteorological Organization, Geneva. OCLC: 778783302.

[Zhao and Gray, 1999] Zhao, L. and Gray, D. M. (1999). Estimating snowmelt infiltration into frozen soils. *Hydrological Processes*, 13(12-13):1827–1842.

[Zhou et al., 2014] Zhou, J., Pomeroy, J. W., Zhang, W., Cheng, G., Wang, G., and Chen, C. (2014). Simulating cold regions hydrological processes using a modular model in the west of China. *Journal of Hydrology*, 509(Supplement C):13–24.